DOI: 10.2478/jlecol-2026-0021 Journal of Landscape Ecology (2026), Vol: 19 / No. 3

MULTI-TEMPORAL ANALYSIS OF FLOOD DYNAMICS AND LAND USE LAND COVER CHANGE IN THE KONAWEHA WATERSHED USING MULTI-SENSOR REMOTE SENSING APPROACH

SEPTIANTO ALDIANSYAH [1,3]*, LAODE MUHAMAD IRSAN [2] AND NUR HASANAH [3]

[1]*Department of Geography, Faculty of Mathematics and Natural Sciences, University of Indonesia, Depok, Indonesia*
[2]*Department of Agrotechnology, Faculty of Agriculture, Gorontalo State University, Gorontalo, Indonesia; laodemuhamadirsan93@gmail.com*
[3]*Department of Geography Education, Faculty of Teacher Training and Education, Halu Oleo University, Kendari, Indonesia; hasanahpatib@uho.ac.id*
**Corresponding author email: septiantoaldiansyah863@gmail.com*

Received: 27th January 2025, **Accepted**: 4th November 2025

ABSTRACT

Flooding is one of the most frequent and destructive environmental hazards globally, and Indonesia is among the most affected countries. Understanding land use land cover (LULC) changes and flood distribution is essential for effective mitigation strategies. However, conventional methods using multiple processing environments are time-consuming, whereas integrating multi-sensor data within a single platform such as Google Earth Engine (GEE) improves efficiency and accuracy. This study aims to analyzes flood distribution and LULC changes in the Konaweha watershed from 2015 to 2024 using multi-temporal Sentinel-1 SAR and Landsat-8 optical imagery. Flooded areas were mapped using the Otsu thresholding combined with change detection, while LULC changes were identified using the Random Forest algorithm. The result reveal that flood inundation expanded from 6,709.24 ha in 2015 to 16,295.35 ha in 2020, before declining to 9,243.28 ha in 2024. Major LULC transitions included reductions in wetlands (12.82 %), primary forest (1.94 %), and agriculture (28.82 %), alongside increase in built-up areas (80.48 %), secondary forest (8.13 %), and water bodies (41.76 %). This finding indicate a strong correlation between flood occurrence and LULC changes, emphasizing the influence of environmental degradation on flood dynamics. The study contributes to global discourse on flood risk assessment by demonstrating the effectiveness of integrating multi-sensor remote sensing data for near real-time flood monitoring and sustainable land management planning.

Keywords: ecosystem; environmental degradation; fragmentation; disaster management; Otsu thresholding

INTRODUCTION

Changes in land use land cover (LULC) indirectly alter environmental conditions, including the hydrological characteristics of an area (Aryal *et al*., 2022). Therefore, LULC studies are often associated with runoff response and flood-related research (Pradhan-Salike & Pokharel, 2017; Pumo *et al*., 2017). Flood frequency has increased over the past few decades and is frequently linked to climate change and landscape morphology. This phenomenon has occurred worldwide, causing material losses, disease outbreaks, and fatalities (Ramakrishna *et al*., 2014; Echendu, 2020). Flooding also indirectly alters LULC by submerging and degrading land, rendering it unsuitable for agriculture. Continuous inundation of farmlands reduces land productivity and food availability (Echendu, 2020; Loc *et al*., 2020; Meyers *et al*., 2021). Such recurring events have been widely reported, including in Indonesia (Ambari, 2013; Handayani *et al*., 2020; Sadeghi *et al*., 2020; Wang *et al*., 2022). Therefore, understanding the impacts of flooding on LULC has become increasingly important (Supari, 2012; Lestari *et al*., 2019).

The Konaweha Watershed frequently experiences severe monthly flooding with a long historical record. These floods not only affect local communities but also disrupt land systems (Marwah, 2014; Kementerian Pekerjaan Umum, 2020a). Between 2013 and 2020, flooding in this region caused extensive material damage, displaced thousands of people, and destroyed hundreds of hectares of agricultural land (Pati, 2013; Antony, 2020; BMKG, 2020; Kementerian Pekerjaan Umum, 2020b). The most severe event occurred in 2000 when river discharge exceeded flood thresholds. These events are primarily driven by prolonged high rainfall intensity, compounded by the watershed's steep topography and extreme weather events caused by rising sea surface temperatures and the convergence of the Australian and Asian monsoon systems (Morse, 2019; BMKG, 2020; Setiawan, 2021). Authorities have responded by constructing levees at the confluence of the Konaweha and Lahumbuti Rivers to mitigate broader impacts (Kementerian Pekerjaan Umum, 2020a), yet these structural measures remain insufficient to fully address the issue.

Although floods are natural phenomena, anthropogenic activities exacerbate their impacts. Disruptions to the hydrological cycle and water availability are also caused by urban expansion, population growth, and LULC changes (Andono, 2014; Gan *et al*., 2018). These conditions increase runoff rates while reducing infiltration capacity (Vaezi *et al*., 2010; Huang *et al*., 2017; Mehr & Akdegirmen, 2021; Naikoo *et al*., 2020; Irham *et al*., 2022). Vegetation plays a crucial role in regulating runoff, infiltration, groundwater recharge, and evapotranspiration rates (van Heerwaarden & Guerau de Arellano, 2008; Smith *et al*., 2015; Devi *et al*., 2019; Puno & Puno, 2019; Srivastava *et al*., 2020; Aghsaei *et al*., 2020; Mehr & Akdegirmen, 2021). These changes ultimately disrupt the balance of the hydrological cycle and river flow distribution (Sahoo *et al*., 2018; Astuti *et al*., 2019; Lacher *et al*., 2019; Li *et al*., 2021b; Silva *et al*., 2021).

Flood vulnerability in the Konaweha Watershed is strongly influenced by LULC change, particularly forest conversion (Tanika, 2013; Gatti *et al*., 2019). Gatti *et al*. (2019) reported that approximately 50 % of the area has undergone LULC change. Such conversions affect the balance between infiltration and runoff (Tang *et al.,* 2020; Oda *et al*., 2021). Kim *et al*. (2019) also found a correlation between LULC change and flood frequency in this region. Moreover, increasing LULC change driven by settlement expansion and infrastructure has transformed large portions of the area (Devi *et al*., 2019; Naikoo *et al*., 2020; Ganaie *et al*., 2021). Urban surfaces dominated by asphalt and concrete further create impervious layers that hinder infiltration (Naikoo *et al*., 2020; Irham *et al*., 2022).

Understanding LULC changes resulting from floods is critical for assessing impacts, evaluating vulnerability, and formulating effective land management strategies. Remote sensing data play an essential role in this context, as both historical and multi-temporal imagery are highly effective for flood identification (Shen *et al*., 2019; Huang & Jin, 2020;

Lechner *et al*., 2020). However, cloud cover remains a major challenge in tropical regions like Indonesia (Huang *et al*., 2018a). Although optical imagery (Acharya *et al*., 2018) and NDWI-based algorithms (Acharya *et al*., 2017; Li *et al*., 2021a; Özelkan, 2020) have shown effectiveness, their accuracy often declines under adverse atmospheric conditions (Amitrano et al., 2018). Alternatively, integrating Synthetic Aperture Radar (SAR) and optical data has been shown to improve multi-scale flood assessments (Martinis *et al*., 2013), automated training data selection (Huang *et al*., 2018b; Westerhoff *et al*., 2013), and observation density during flood events (Chaouch *et al*., 2012). Despite the variety of methods for flood monitoring using SAR data, few studies have leveraged stacked SAR or optical time-series imagery due to challenges in accessing and processing large datasets.

The open data policies of NASA–USGS and Copernicus, combined with cloud-based platforms such as Google Earth Engine (GEE), have facilitated the exploration of methods utilizing complete satellite archives to enhance observation-based flood monitoring systems. Numerous studies have demonstrated the effectiveness of SAR and Landsat imagery in identifying floods and their relationship with LULC (Barredo & Engelen, 2010; Rawat & Kumar, 2015; Hua, 2017; Liping *et al*., 2018; Amitrano *et al*., 2018; Uddin *et al*., 2019; Nguyen *et al*., 2020; Talukdar *et al.,* 2020; Idowu & Zhou, 2021; Banjara *et al*., 2024). Research in Pordenone Province, Italy, highlighted population growth and urbanization as key drivers of declining natural vegetation cover (Barredo & Engelen, 2010), while studies in the Philippines revealed weakened soil capacity to prevent flooding due to land conversion (Boardman *et al.,* 2019).

Historically, flood extent in the Konaweha Watershed has been estimated conventionally rather than derived from spatially explicit data. Accurate information from comprehensive research depends on data quality and analytical depth (Dalanhol *et al*., 2020). Previous studies in this watershed have focused on specific hydrological aspects such as river discharge (Surya *et al*., 2014; Jasman *et al*., 2023; Maladeni *et al.,* 2023), long-term hydrological simulations and projections (Tanika, 2013), and regional vulnerability assessments (Baco *et al*., 2014). However, these studies have not provided a detailed linkage between flood events and land cover dynamics (Tanika, 2013; Setiawan, 2021; Jasman *et al*., 2023).

This knowledge gap limits empirical understanding of the actual relationship between LULC change and flooding in the Konaweha Watershed—particularly through data that can be rapidly accessed and analyzed on GEE. Historically, most areas within the watershed have not been well mapped. Therefore, this study examines the extent and characteristics of LULC changes and maps flood inundation areas in the Konaweha Watershed using Sentinel-1 SAR and Landsat archives within the GEE environment. The findings provide valuable insights for policymakers, decision-makers, and regional planners, offering crucial information for flood vulnerability mapping, early warning systems, and evacuation planning in the future.

MATERIALS AND METHODS

Study Area

This research was conducted in the Konaweha Watershed in Southeast Sulawesi Province (Fig. 1). The Konaweha watershed has an area of 697,947.51 ha and is the largest watershed in Southeast Sulawesi Province. This watershed has a strategic function and administratively covers four autonomous regions: Konawe Regency, South Konawe Regency, Kolaka Regency, and Kendari City. Floods hit this area, affecting 4000 people in 50 villages in 2020 (Rakyat, 2020; Fig. 2). Apart from submerging dozens of houses, the flood also caused agricultural land to be submerged and damaged (Tamenk, 2021). The steep topographic conditions of the watershed and the short transition zone provide a greater opportunity for flooding phenomena to occur due to high rainfall intensity (Setiawan, 2021).

Fig. 1: Location of the study area: Sulawesi (a), Southeast Sulawesi (b), Konaweha Watershed (c) and (d), Satellite image of the study area in CIR band combination in 2020 (c), DEM map showing elevation of the study area (d).

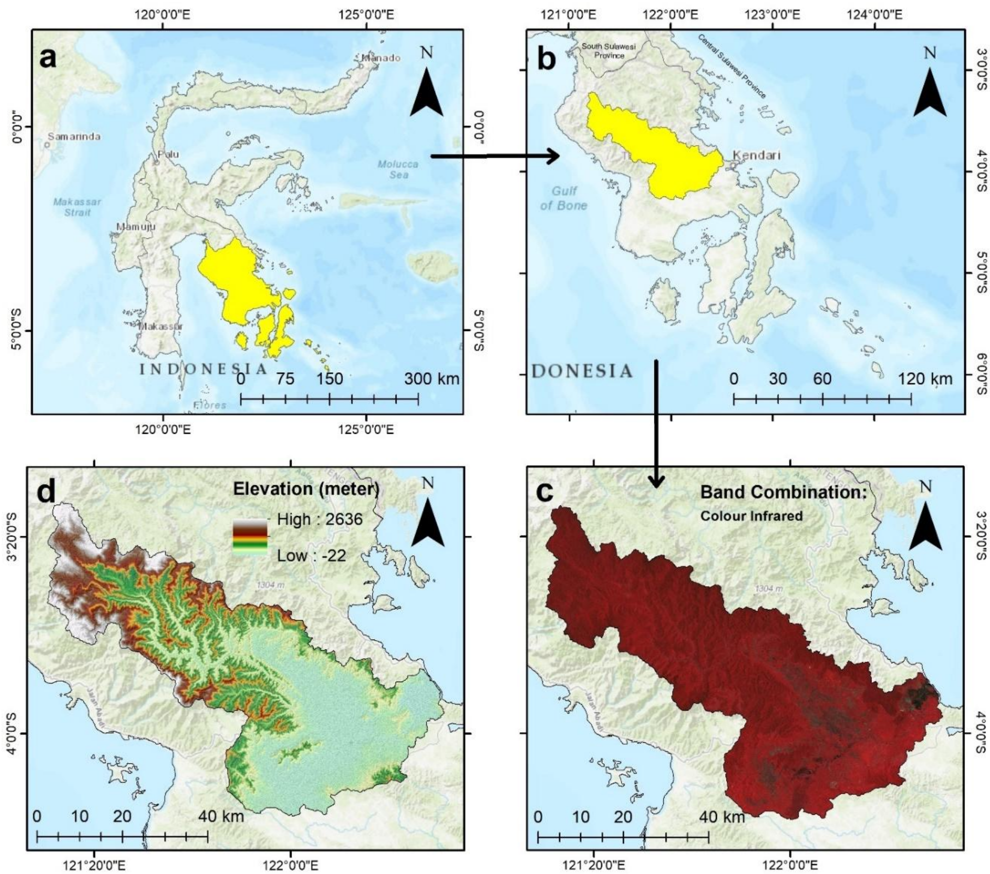

Data Availability

The research data were obtained from radar and optical imagery openly available through the GEE platform. The selection of Sentinel and Landsat imagery was adjusted to documented flood events and the availability of satellite observations representing baseline, intermediate, and recent conditions. Specifically, the radar data consist of Sentinel-1 VV mosaics for June–July 2015, July 2019, July 2020, and April–May 2024, while the optical data consist of Landsat-8 mosaics for 2015, 2020, and 2024. The 2024 dataset represents actual satellite acquisitions rather than predictions. The selection of these years was based on two criteria: 1) temporal correspondence with flood events documented through reports and news sources in the study area, and 2) the availability of imagery with sufficient quality after mosaicking and cloud masking (Peña-Luque *et al.*, 2021; Tarpanelli *et al.*, 2022; Johary *et al.*, 2023).

Fig. 2: Floods submerged residential areas in Laloika Village and Wonuamonapa Village (top left), Wonuamonapa Village (top right), Anggoro Village (bottom left), and floods reached the base of the Rahabangga Bridge in Uepai District (bottom right) (Witanto, 2019; Rakyat, 2020).

For radar data, the Sentinel-1 polarization used was VV, as it produces more stable backscatter (Zhang *et al*., 2016), enables better discrimination between water and non-water surfaces compared to VH polarization (Chulafak *et al*., 2021), and is more suitable for tropical vegetation conditions in Indonesia (Zhang *et al.,* 2020). Meanwhile, Landsat-8 was selected because its sensor provides medium spatial resolution with broad spectral coverage (Blue, Green, Red, Near-Infrared, Short-Wave Infrared 1, and Short-Wave Infrared 2 bands), which is effective for analyzing LULC changes. In addition, the Landsat-8 series offers a long-term archive with strong radiometric consistency, making it highly suitable for the multi-temporal analysis required in this study.

Flood Analysis

Flood Inundation Detection

Sentinel-1 VV imagery is used to map flood inundation, while GEE is used to process the data. The pre-processing stage is carried out by preparing input data to determine the threshold and detection of flood inundation. This stage begins by focusing the area on the study location, namely the Konaweha Watershed in Southeast Sulawesi Province to speed up processing, Sentinel-1 image speckle noise correction, determining the difference in backscatter values, and detecting permanent water bodies from Sentinel-2 images. To eliminate speckle noise in the image, a 3x3 median filter is used to produce a better signal-to-noise (Cao *et al*., 2019).

Permanent water bodies are then detected by performing the Sentinel-2 mosaic image using the automatic water extraction index (AWEI) concerning pixel values greater than -0.232 (Papila *et al.*, 2020). Permanent water bodies are used to mask permanent water bodies so that they can be removed from Sentinel-1 images. This aims to minimize errors in flood detection results. Then the calculation of the difference in the mixed values is carried out. The difference in scattering values is calculated by subtracting the post-flood data from that collected before the flood.

The Otsu thresholding algorithm was applied to automatically determine an optimal threshold value t for separating water and non-water pixels from the Sentinel-1 VV backscatter intensity histogram. The method identifies the threshold that maximizes the inter-class variance between two classes, equivalent to minimizing the intra-class variance (Otsu, 1975). This approach has been widely demonstrated as a simple and effective technique for surface water mapping (e.g., Papila *et al.*, 2020; Cao *et al.*, 2019). For each pre-processed Sentinel-1 VV image in the time series, the algorithm searches exhaustively across all possible thresholds and selects the one that best partitions the histogram into water and non-water classes. Pixels with backscatter values lower than the estimated threshold were classified as water, whereas values greater than or equal to the threshold were classified as non-water.

$$\begin{Bmatrix} \delta^2 = P_{nw}(M_{nw} - M)^2 + P_w(M_w - M)^2, \\ M = P_{nw}M_{nw} + P_w M_w, \\ P_{nw} + P_w = 1 \\ Th_{Otsu} = Arg \underset{x \leq Th_{Otsu} \leq y}{max} (\delta^2) \end{Bmatrix} \quad \text{(eq.1)}$$

where, δ^2 is the variance between classes of water bodies and non-water bodies; M_{nw} and M_w are the average pixels of non-water bodies and water bodies; P_{nw} and P_w are the probabilities of pixels belonging to the non-water-body or the water-body class; M is the average of the entire image.

Mapping of Land Use Land Cover Changes

LULC changes were extracted using the change detection method. The post-classification comparison (PCC) approach is applied to identify LULC changes (Tiede, 2014; Priyatna *et al.*, 2023). A pixel-based integrated digital classification method was used to classify LULC types from Landsat-8 satellite imagery. The types of LULC were classified into nine classes, namely built-up, bareland, water body, wetland, primary forest, secondary forest, shrub, palm oil, and agriculture (Table 1). The classification of LULC is summarized based on SNI 7645-2014 (Badan Standardisasi Nasional, 2022) regulations regarding the classification of LULC based on regional geomorphology. Before classification, the visible and near-infrared spectral bands were combined to produce a multispectral image. The color infrared band (CIR) combination is used as a standard false color composite to facilitate LULC interpretation and differentiation. CIR is obtained by combining the near-infrared, red, and green bands. This combination was chosen to facilitate the detection of vegetation in images based on spectral reflectance properties with vegetation appearing in various shades of red. The soil will appear in different brown colors, while urban or built-up areas will have a cyan-blue or yellow/gray color according to their composition. The water will be dark bluish (clear water) and greenish blue (murky water) due to sediment reflection (Fig. 1c).

Training data was collected on a polygon basis for each class. Data were identified through composite visual interpretation and then converted into sample points through stratified random sampling. The number of samples used for LULC identification in 2015, 2020, and 2024 was 12,316, 15,592, and 15,902, respectively. The dataset was randomly split into 80 % training and 20 % validation subsets. Accuracy assessment was performed using the independent validation subset, confusion matrices, overall accuracy (OA), and Kappa statistics.

The Random Forest (RF) classification algorithm with a prediction tree of one hundred was used in this research. The RF algorithm is a classifier that consists of a combination of prediction trees and depends on the value of each sample vector (Breiman, 2001). This algorithm was chosen considering its efficiency in classifying LULC in an area (Akar & Güngör, 2012). This algorithm is considered superior to other classification methods in terms of sample calculation speed, stable parameters, and high accuracy (Pelletier *et al*., 2016). A combination of bootstrap aggregation (bagging) with random feature sorting is done to create a set of controlled variance decision trees. This study uses two sets of parameters, namely the number of parameters, and the depth of the decision trees to improve classification accuracy. The depth of the decision trees is determined based on the number of features used to slice the nodes. The node impurity of the tree is evaluated by Gini (G), which is formulated using equation 2 (Breiman, 2001):

$$E = 1 - \sum_{i=1}^{c} p_i^2 \qquad \text{(eq.2)}$$

where p_i is a probability of a pixel being classified. Parameter optimization was performed using the GridSearchCV method on scikit learn (Pedregosa *et al*., 2011). Based on the results of hyperparameter tuning, the maximum depth of trees found is 10, the minimum number of samples required to beat a leaf node is 4, the minimum number of samples required to split an internal node is 8 and the number of trees was set as 100.

Table 1: LULC classes used in the study and their corresponding description

Class	Description
Built-up	Land that has undergone a development or paving process.
Bareland	Land that cannot be cultivated and transition areas (agricultural land to built-up areas), including beaches, exposed rocks, and open land.
Waterbody	Freshwater bodies such as rivers, ponds, lakes, and so on.
Wetland	A land where the soil is saturated with water, either permanently or seasonally, such as swamps, brackish, and peat.
Primary forest	Forests with native vegetation develop as a result of natural disturbances and natural processes, without anthropogenic disturbance.
Secondary forest	Forests that have regenerated naturally after anthropogenic disturbance and transition areas (forest to agricultural land/plantations)
Shrub	Land covered with low plants close to the ground surface.
Palm oil	Cultivated plants with a distinctive rough texture, regular pattern, and star-shaped crown.
Agriculture	Agricultural land includes fruit orchards, horticultural land, and agricultural land that has not been cultivated < 1 year.

Mapping the distribution of flood inundation

Mapping the distribution of flood inundation locations was carried out using the overlay technique. Overlay is the application of multi-criteria to the data layer (Faisal & Shaker, 2017). The results of identifying flood inundations using the Otsu thresholding are overlaid with the classification of LULC in 2015, 2020, and 2024. In this way, we can see the distribution of flood inundation locations for each form of LULC used in the study location.

Accuracy Assessment

It is important to carry out an accuracy assessment to verify and validate the results of LULC classification. This is done by comparing the classification map with a reference map from Google Earth Pro (Baccari *et al*., 2025). We created a confusion matrix and calculated the OA, user accuracy (UA), and producer accuracy (PA) of the classification results to determine potential errors in the classification process (Baccari *et al.,* 2025). This is done by generating a series of random points from the reference map with a number adjusted to the relative area of each class. Accuracy assessment is also assessed from the k Coefficient. This is a statistical measure of association that is commonly used in assessing suitability or accuracy in classification (Talukdar *et al*., 2020). Accuracy assessment aims to be a quantitative indicator of the quality of classification results by considering the error matrix and is defined in terms of errors (Talukdar *et al*., 2020). The following OA and kappa formulas are used to calculate the accuracy of each classification map:

$$OA = \left(\frac{Pc}{Pn}\right) * 100 \quad \text{(eq.3)}$$

where Pc is the number of pixels classified correctly and Pn is the total number of pixels.

$$\mathrm{k} = \frac{N \ \sum_{i=1}^{r} x_{ii} - \sum_{i=1}^{r} (x_{i+} \ x \ x_{+i})}{N^2 - \sum_{i=1}^{r} (x_{i+} \ x \ x_{+i})} \quad \text{(eq.4)}$$

where *r* = the number of rows and columns in the error matrix, x_{ii} = the number of observations in row *i* and column *i*, x_{i+} = the marginal total of row *i*, x_{+i}= the marginal total of column *i*, and *N* = the total number of observations.

The same procedure was applied to the flood inundation map. Validation was conducted by comparing Sentinel-2 and Sentinel-1 to record flood inundation conditions in July 2015, 2020, and May 2024. Due to the high cloud coverage in the Sentinel-2 images during these months, cloud masking was performed using the QA60 band (Carrasco *et al*., 2019; Sun *et al*., 2025). In this process, cloud and cirrus pixels were masked and replaced using cloud-free observations from adjacent times to improve the reliability of the reference data. Subsequently, the initial cloud-covered areas in Sentinel-2 were sampled using Sentinel-1 images as an alternative source of reference data. This approach ensures that the reference data for flood inundation validation remain consistent even in cloud-contaminated regions.

McHugh (2012) and Talukdar *et al.* (2020) stated that the results of the kappa value can be interpreted as follows: A kappa value <0.40 indicates poor agreement, a value between 0.40 and 0.55 indicates fair agreement, a value with an interval between 0.55 and 0.70 indicates good agreement, a value between 0.70 and 0.85 indicate very good agreement, and values >0.85 indicate excellent agreement. The flowchart of the methodology is shown in Fig. 3.

Fig. 3: Overall methodological framework for mapping and assessing land use of flood-affected land cover using Sentinel-1 and Landsat-8 satellite imagery.

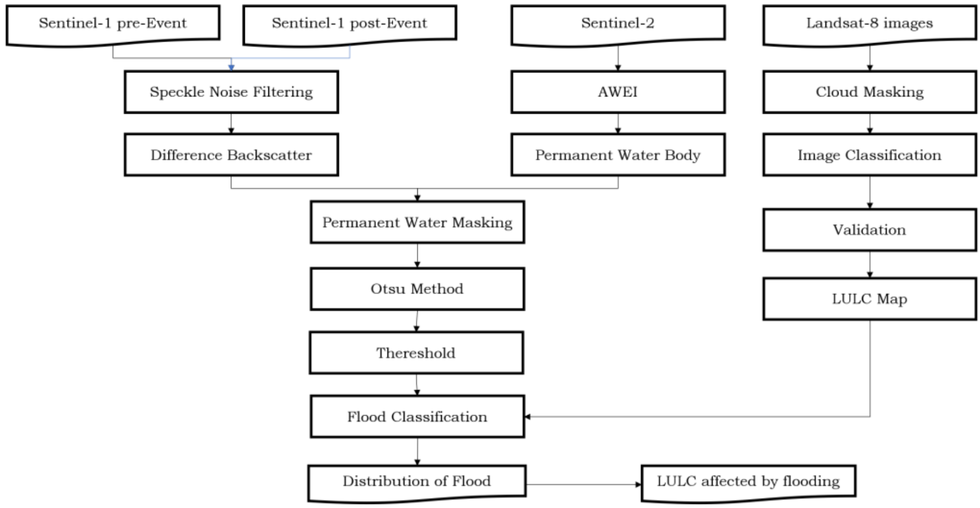

RESULT

Flood Inundation

The application of the Otsu thresholding in this study was able to detect flood inundation area with good performance. Most of the flood inundation were located in the downstream areas of the Konaweha Watershed. The flood inundation areas mapped in 2015, 2020, and 2024 were 6,709.24 ha, 16,295.35 ha, and 9,243.28 ha, respectively. The distribution of flood inundation showed significant spatial dynamics during the 2015–2024 period. In 2015, the inundation was recorded at 3,431.30 ha, then increased sharply in 2020 to 13,382.83 ha, indicating an expansion of the flood-affected area. However, in 2024, the flood inundation area decreased to 4,657.06 ha, which could indicate improvements in the drainage system, mitigation efforts, or drier climate variations compared to the previous period. During 2015–2020, flood inundation expanded from the initial flood epicenter to a new area of 563.74 ha, while the 2020–2024 period shows persistence and spatial shifts in inundation after the peak event of 1,841.45 ha. The area experiencing the same flood inundation between 2015 and 2024 was 2,321.89 ha, while the flood inundation area across the entire period was 312.76 ha. Based on its distribution in the sub-district area, the widest flood distribution in 2015 was in the Wonggeduku Barat (9.81 %), Motui (9.79 %), and Uepai (9.59 %) sub-districts. Meanwhile, the flood distribution >5 % of the area was Wawotobi (6.82 %) and Wonggeduku (5.05 %). Other areas were in <5 % of the area. In 2020, the percentage of flood distribution mentioned in the previous period decreased, except for Wonggeduku (13.63 %), which experienced an increase in area. Other new areas that experienced an increase in flood distribution were Tongauna (11.90 %), Pondidaha (11.77 %), and Ladongi (10.94 %). Meanwhile, Angata experienced an increase up to 5.23 % of its sub-district area. In 2024, Ladongi recorded the highest flood inundation proportion (15.47 %), while, Wonggeduku and Pondidaha showed a decline to 6.43 % and 6.40 %, respectively. Flood inundation also expanded to Motui in 2024, reaching 6.08 % of its area. The identified flood inundation areas can be seen in Fig. 4. Meanwhile, the proportion of flood inundation per sub-district is shown in Fig. 5.

Fig. 4: Flood inundation from Sentinel-1 imagery using the Otsu thresholding.

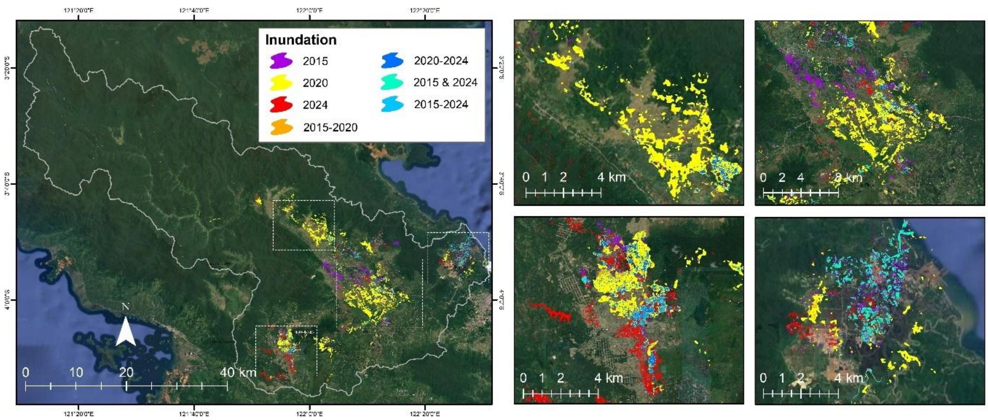

Fig. 5: Flood inundation based on sub-district area.

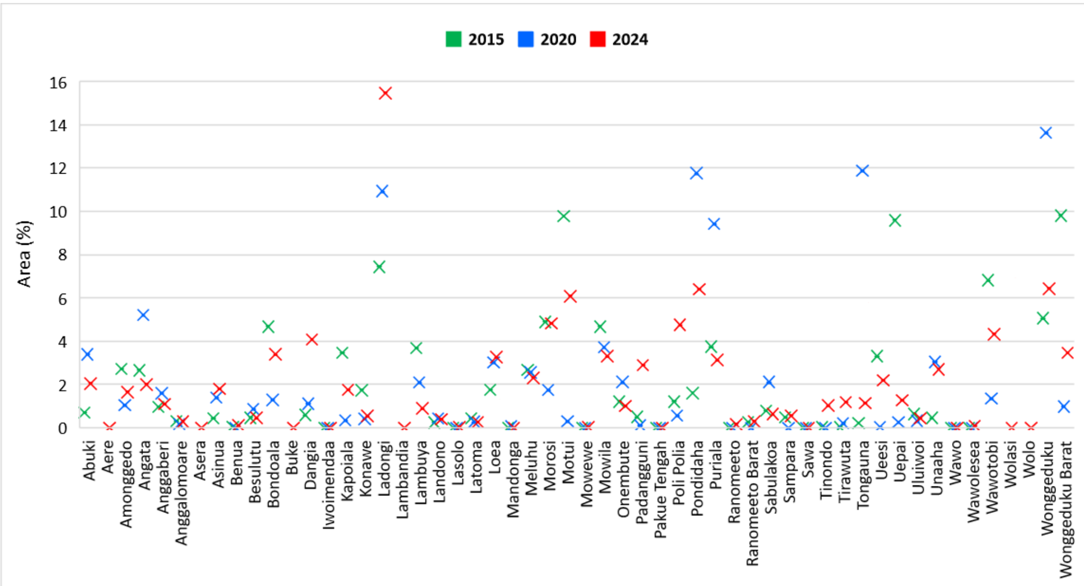

Land Use Land Cover Changes

Changes in LULC within the Konaweha Watershed showed clear shifts in land cover between 2015 to 2024 (Fig. 6). The results of the research show that over ten years there has been a decrease in the area of wetland (-832.04 ha), primary forest (-7,836.50 ha), and agriculture (-32,515.43 ha). Conversely, an expansion of secondary forest was observed, reaching 14,120.16 ha.

Fig. 6: Spatial and quantitative in land use land cover changes in the Konaweha watershed during 2015–2024

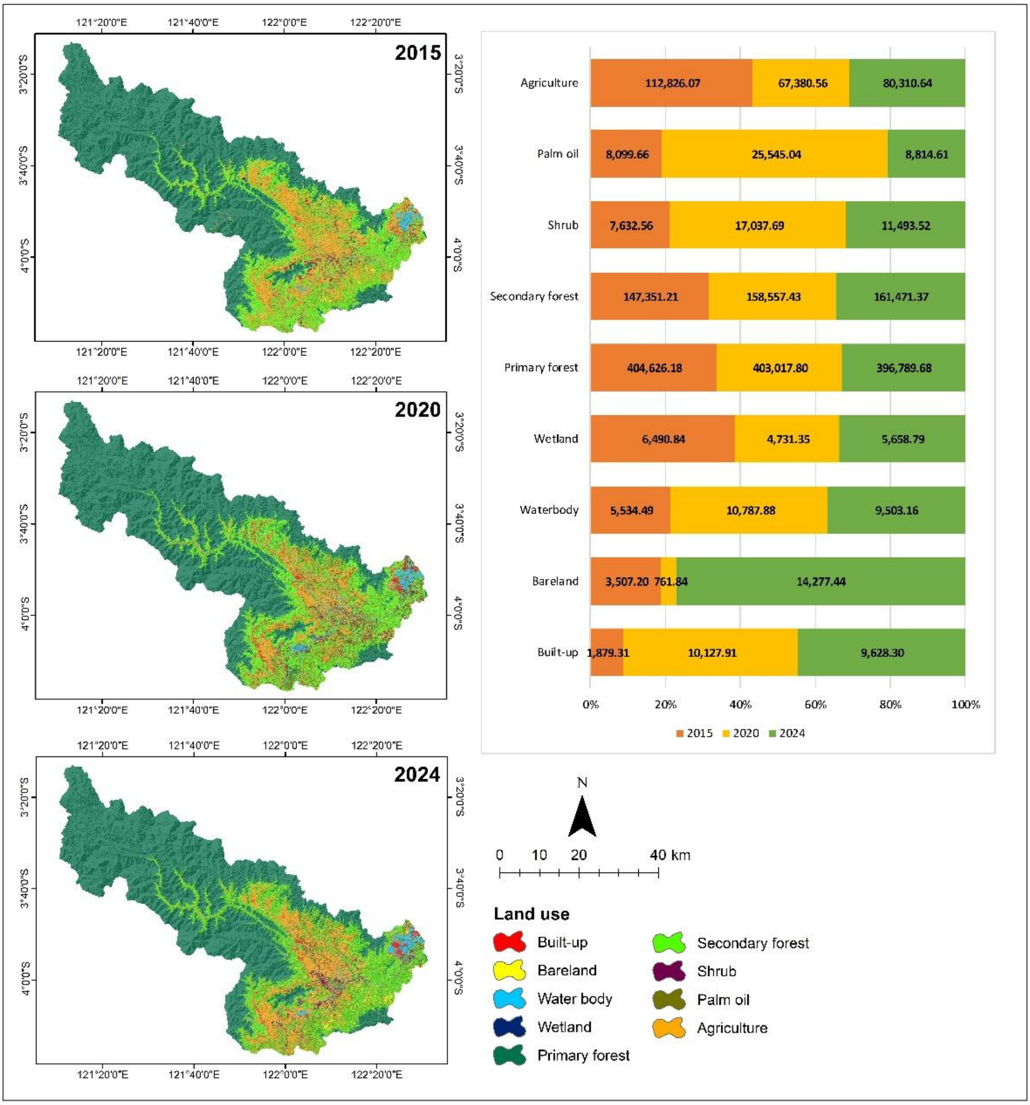

In 2024, the Konaweha Watershed was still dominated by primary forest (56.85 %) and secondary forest (23.14 %), indicating that forest cover still accounted for 79.99 % of the watershed area. In addition, increases in built-up land (7,748.30 ha), bare land (10,770.24 ha), water bodies (9,503.16 ha), shrubs (11,493.52 ha), and palm oil plantations (714.95 ha) were recorded. These changes indicate a shift from natural and agricultural land covers towards more human-modified and transitional LULC types within the Konaweha Watershed.

Accuracy Assessment

Fig. 7 shows the error matrix consisting of OA, PA, UA, and kappa coefficient. The OA of the two LULC maps in 2015, 2020, and 2024 is 96.65 %, 97.93 %, and 97.66 %, respectively. The corresponding kappa values for the same years were 0.86, 0.83, and 0.85, respectively. The detailed classification accuracy matrix calculation is shown in Appendix Table A.

In addition, accuracy measurements were conducted to display the performance of flood inundation detection by comparing the results of the Otsu threshold from Sentinel-1 using observations from Sentinel-2. Overall classification accuracy showed values of 90.10 %, 91.74 %, and 93.36 % respectively with kappa coefficients of 0.74, 0.79, and 0.86. The accuracy of each class is illustrated in Fig. 8. This high-accuracy result shows the performance of the Otsu thresholding in distinguishing water and non-water pixels. These results demonstrate that both the LULC classification and the flood inundation mapping achieved high accuracy and strong agreement, confirming the suitability of the applied methods in identifying LULC dynamics and flood-affected areas in the study region.

Fig. 7: User and producer accuracy on land use land cover map

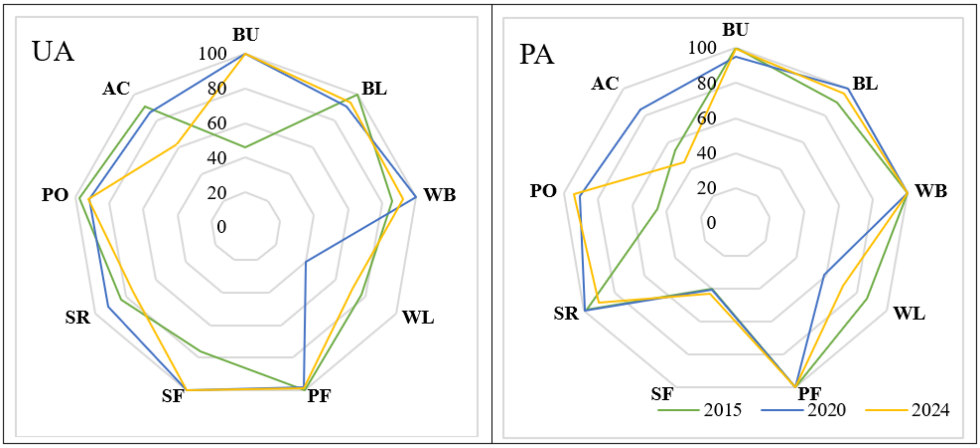

Fig. 8: User and producer accuracy on Flood Inundation

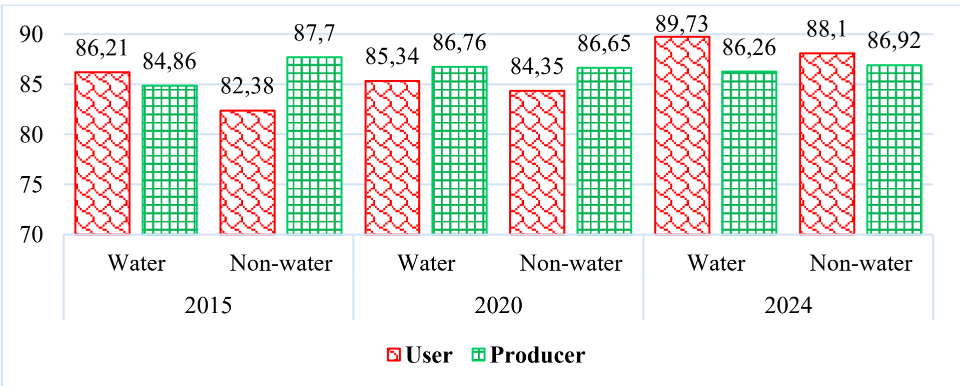

The Distribution of Flood Inundation

The flood inundation distribution map is produced by overlaying the flood inundation and LULC maps. The highest proportion of flood inundation was spread over agriculture land in 2015, 2020, and 2024, covering an area of 64 %, 64 %, and 61 %, respectively. Water bodies also have a fairly large proportion, reaching 27 %, 11% and 23 %, respectively. Meanwhile, flood inundation over built-up areas slightly increased from 0.93 % in 2015 to 2.15 % in 2020 and 2.98 % in 2024. A more informative distribution of flood inundation is presented in Fig. 9.

Fig. 9: Distribution of flood inundation in the Konaweha watershed

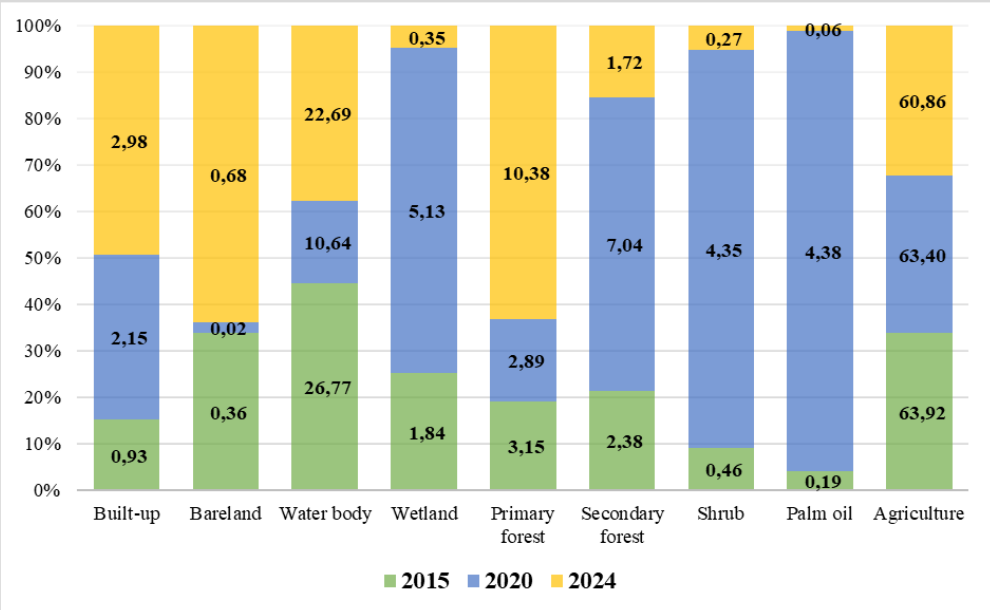

DISCUSSION

Flood Inundation

Sentinel-1 SAR has been widely used in water resources management studies, particularly in tropical and humid regions. This satellite is advantageous because it can penetrate clouds, has a spatial resolution of 10 m, and offers relatively frequent revisit times (Rucci *et al.,* 2012; Plank, 2014). However, its use for detecting flood inundation remains very limited in the Konaweha Watershed. The complex morphology of the Konaweha Watershed makes the area vulnerable to hydrological system changes and global climate dynamics (Tessler *et al*., 2015; Veettil *et al*., 2019; Triet *et al.,* 2020).

In this context, the Otsu thresholding was applied to determine flood thresholds adaptively based on the backscatter values (σ^0) of Sentinel-1 SAR imagery in decibel (dB) units, rather than using optical indices like NDWI. The threshold values obtained for 2015, 2020, and 2024 were −2.53, −2.74, and −2.41, respectively. Pixels with values below these thresholds were identified as flood inundation areas. Such negative values are common in radar-based analysis because backscatter values typically range from −25 to +5 dB, depending on surface conditions and incidence angle (Manjusree *et al*., 2012; Tran *et al*., 2020; Moharrami *et al*., 2021; Lang *et al*., 2024).

Differences in threshold values across years reflect variations in surface conditions, vegetation, and soil moisture, which affect backscatter, making the use of a single annual threshold inadvisable (Pham-Duc *et al*., 2017). Moreover, high backscatter values in permanent water bodies may be influenced by dissolved particles that increase surface roughness and radar reflectivity (Purinton & Bookhagen, 2020). The Konaweha Watershed, with its complex morphology and dense vegetation, exhibits large temporal variations in backscatter, with turbulence and suspended particles affecting inter-water body reflection values (Purinton & Bookhagen, 2020).

These results are consistent with studies showing that VV polarization backscatter intensity tends to be lower during the dry season than the wet season. Therefore, applying a dynamic Otsu thresholding is more adaptive than a static approach, as it can adjust to temporal variations in vegetation and surface moisture (Tran *et al*., 2020; Moharrami *et al*., 2021; Priyatna *et al*., 2023; Lang *et al*., 2024). This study demonstrates the reliability of the Otsu thresholding in detecting floods inundation in areas with high variability, although limitations in validation and spatial accuracy remain challenges. The irregular frequency of flood events and the large area make integrated approaches difficult to implement for near-real-time monitoring.

Although this study did not perform a quantitative comparison between multi-sensor and single-sensor approaches, improved detection reliability was obtained from the spatial consistency of classified results and the correspondence of inundation patterns with field reference data and optical imagery. Thus, the claim of the superiority of the multi-sensor approach in this study is qualitative and supported by previous literature demonstrating increased accuracy in areas with heterogeneous LULC and high moisture (Tran *et al*., 2020; Moharrami *et al*., 2021; Lang *et al*., 2024).

The spatiotemporal dynamics of flood inundation in the Konaweha Watershed exhibit fluctuating patterns, reflecting a dynamic hydrological response. The increased flood inundation area in 2020 was likely influenced by high rainfall intensity, LULC changes, and decreased vegetation cover, whereas the decrease in 2024 may be related to improved drainage systems, mitigation efforts, or relatively drier climatic conditions. Consistent flood inundation in some districts, such as Wongeduku and Ladongi, indicates the vulnerability of these areas to annual flooding.

Flooding in the Konaweha Watershed also has significant socio-economic impacts. According to BNPB (2021), Konawe Regency experienced the highest physical and economic losses in Southeast Sulawesi Province, reaching IDR 4.86 trillion and IDR 5 trillion, respectively. These impacts include reduced agricultural productivity and increased post-disaster recovery costs, as similarly reported in other tropical regions such as Vietnam and Thailand (Triet *et al*., 2020; Veettil *et al.,* 2019). Therefore, integrating flood inundation detection results with disaster risk management policies is crucial for minimizing social and economic losses.

Nevertheless, the observed increase in detected water bodies should be interpreted cautiously, considering variations in accuracy among classes. Some classes, such as wetlands and agricultural land, show relatively low UA. This is likely due to spectral similarity and backscatter characteristics between flooded rice fields, swamps, and water bodies, as well as landscape mosaics and limitations in field reference data, increasing the potential for commission and omission errors.

These findings align with Zhang *et al*. (2023), showing that while long-term wetland accuracy is generally high, specific errors may occur in fragmented mixed landscapes. Therefore, some detected changes may reflect real dynamics, while others may result from misclassification, especially in areas with high moisture or temporary inundation (Deng *et al*., 2023; Zhang *et al*., 2024). Based on validation results, classification errors are estimated not to exceed 10 %, and thus do not significantly affect the interpretation of main spatial patterns. However, this uncertainty remains an important limitation and should be considered in further analyses using higher-resolution data.

Climatologically, variations in flood inundation in the Konaweha Watershed are closely related to regional weather and climate dynamics. Several local studies (Erna *et al*., 2021; Andono *et al*., 2014; Baco *et al.,* 2017) and global studies (Torre Zaffaroni *et al*., 2023; Hariadi *et al*., 2023) indicate that rainfall intensity and duration, as well as air temperature, significantly affect flood inundation extent through increased surface runoff, especially in areas with suboptimal and poorly permeable drainage systems.

Rainfall and temperature data from BMKG also show that flood inundation periods in the Konaweha Watershed generally coincide with significant rainfall increases compared to dry season months, while air temperatures tend to be lower during these periods (BPS, 2015a,b; 2019a,b; 2020). These findings provide climatological context that supports the interpretation of observed spatial changes in flood inundation extent.

Overall, the results indicate that the combination of hydrometeorological influences, LULC changes, and radar backscatter characteristics plays a crucial role in determining flood inundation detection accuracy in the Konaweha Watershed. The Sentinel-1 SAR–based approach and Otsu thresholding provide a solid foundation for long-term flood inundation monitoring, although improved validation and integration of climatological variables are still necessary to support more comprehensive hydrological risk analyses.

Land use land cover dynamics

The degradation of primary forests and the expansion of secondary forests in the Konaweha Watershed indicate that, although overall forest cover remains high (79.99 %), the functional roles of these two forest types in regulating hydrology differ significantly. Primary forests have more complex canopy structures, thick litter layers, and deep root systems that contribute to water infiltration and surface runoff control. In contrast, secondary forests, which regrow after disturbances, generally have lower water retention capacity and are not fully able to stabilize surface flow. Substantial loss of primary forests can increase runoff and reduce infiltration capacity, ultimately amplifying flood potential in downstream areas.

LULC analysis shows that land conversion to built-up areas reached 7,748.99 ha, potentially exacerbating disturbances to hydrological balance. Population growth further increases land pressure through settlement expansion, agricultural land opening, and intensified food production (Abdo, 2018; Rahmoun *et al*., 2018). This situation reflects LULC change in strategies aimed at reducing economic losses but often accelerates environmental degradation (Kelley & Prabowo, 2019; Arfanuzzaman & Dahiya, 2019).

These findings are consistent with studies in other tropical watersheds, showing that primary forest degradation correlates with increased surface runoff, decreased groundwater retention capacity, and more extreme hydrological responses to rainfall (Birhanu *et al*., 2019; Deng *et al.,* 2023; Mukaddas *et al*., 2023; Zhang *et al*., 2024). This underscores the importance of maintaining the quality and continuity of primary forest cover as a key regulator of hydrological regimes in the Konaweha Watershed.

Therefore, LULC change in the Konaweha Watershed not only reflect ecological dynamics but also highlight complex interactions between social and economic factors. Control measures are needed to minimize inter-regional disparities through LULC regulation enforcement (Calder *et al*., 2006; Lee & Brody, 2018). Approaches such as vertical housing development and sustainable environmental design can help preserve the functions of the catchment area. Although this study is limited to identifying inundation locations, its results provide an important basis for understanding the relationship between LULC patterns and flood risk. Future research should integrate topographic and rainfall variables to identify key drivers, as floods are also influenced by meteorological, ecological, and policy factors (Nie *et al*., 2012).

The Konaweha Watershed case supports global observations that forest quality is as important as forest quantity in regulating flood risk. While maintaining forest areas remains crucial, preserving forest ecological integrity provides greater hydrological stability than merely increasing secondary vegetation cover. These findings align with studies showing that tropical catchments with higher primary forest retention experience lower peak flow fluctuations, even under varying rainfall regimes (Karlson *et al*., 2023; Deng *et al*., 2023).

However, direct attribution between LULC change and flood occurrences in this study remains indicative, as predictive hydrological or rainfall modeling was not applied. This study uses a retrospective approach to trace historical LULC changes rather than project future flood scenarios. Such an approach remains relevant for understanding historical LULC transitions without requiring explicit hydrological models (Zhang *et al*., 2024). Nonetheless, future studies are recommended to integrate hydrological modeling and LULC change scenarios to more accurately quantify the impact of land changes on flood dynamics in the Konaweha Watershed.

From a landscape ecology perspective, map overlays reveal that flood impacts are most pronounced in the agricultural sector. Most flood inundation areas in 2015, 2020, and 2024 were agricultural land, approximately 64 %, 64 %, and 61 %, respectively. This indicates high vulnerability of the agricultural sector to floods, with implications for food security. Studies in Africa report that 12 % of the population is food insecure due to flooding (Reed *et al.,* 2022), while in Nigeria and Malaysia, floods reduce land efficiency and farmers' income (Soulibouth *et al.,* 2021; Jega *et al*., 2018). Increased flood frequency and intensity exacerbate erosion, water contamination, and soil degradation, while climate change intensifies risks through extreme rainfall events (Tabari, 2020). This underscores the need for landscape-ecology-based mitigation strategies that integrate forest conservation, wetland rehabilitation, and regulation of agricultural land use in flood-prone areas. Stakeholder collaboration is also essential to balance productivity and conservation.

Beyond agriculture, flood dynamics also impact aquatic ecosystems and built-up areas. Inundation proportions in water bodies reached 27 %, 11 %, and 23 % in 2015, 2020, and 2024, respectively, potentially affecting biodiversity and ecological functions of aquatic systems (Ochoa-Sánchez *et al.,* 2022). Therefore, flood management should consider aquatic ecosystem aspects comprehensively. Meanwhile, built-up areas experienced relatively small inundation (0.93–2.98 %) but significantly affected infrastructure and transportation. This emphasizes the importance of implementing efficient drainage systems and green technologies as part of urban flood mitigation (Kundzewicz *et al*., 2014; Iturriza *et al*., 2020; Akaolisa *et al*., 2023).

Policy Implementation

Integration of flood inundation mapping with LULC data shows that flood inundation occurs predominantly in areas that are vital for ecosystem functions and human safety. These findings underscore the need for BNPB and BPBD to adopt SAR-based flood inundation maps into regional risk mapping systems such as InaRISK and InaSAFE, to support near-real-time flood inundation monitoring that is not hindered by cloud cover. This approach has been effectively implemented in Bangladesh and Vietnam to enhance emergency planning and agricultural loss assessment (Uddin *et al.,* 2019; Nguyen *et al.,* 2023; Singha *et al*., 2020).

The expansion of built-up areas and the reduction of vegetation cover in the midstream and downstream regions indicate the need for stricter LULC control in flood inundation-prone zones. Regional Development Planning Agency and Department of Environment should establish adaptive drainage standards and maintain green open spaces in impervious areas to enhance infiltration and slow surface runoff. Practices in Thailand and Malaysia have demonstrated the effectiveness of zoning in reducing urban flood inundation frequency (Islam & Meng, 2022; Tavus *et al*., 2022).

In the upstream and midstream parts of the watershed, loss of forest cover and expansion of dryland agriculture exacerbate erosion and sedimentation, increasing downstream flood inundation risk. Therefore, riparian vegetation rehabilitation and riverbank reforestation should be prioritized, supported by ecosystem restoration policies based on watershed management. Studies in the United States indicate that riparian vegetation rehabilitation can significantly reduce peak flood inundation discharge and enhance baseflow (Gay *et al*., 2023).

The development of semi-automated workflows based on Sentinel-1 in GEE can strengthen BPBD's early warning systems, particularly during extreme rainfall events. Training BPBD personnel and village officials in SAR data interpretation is also necessary to enhance community preparedness (Destana). This approach can improve flood detection accuracy and reduce response times, delivering timely alerts to communities (Wania *et al*., 2021). Additionally, ecosystem-based adaptation strategies can provide an efficient and sustainable mitigation option, capable of reducing combined inundation from river runoff (Pelckmans *et al*., 2024).

Limitations and potential improvements

Although the Otsu thresholding and the GEE platform can monitor flood inundation near real-time, several limitations require further investigation. First, land surface dynamics can alter temporal Z-score values. For instance, the loss of forest canopy or crops may be associated with changes in SAR backscatter when scattering shifts from volumetric canopy to bare soil surfaces (Shimada *et al*., 2014). These differences may be substantial enough to produce anomaly scores, although they are usually not identical to open surfaces (Cian *et al*., 2018). In most cases, such dynamics can arise from regular flood inundation patterns, such as frequently flood inundation rice fields, complicating the selection of a non-flood inundation baseline. This condition allows only dry-season imagery to be used for the Sentinel-1 baseline period and other SAR archives, enabling the exclusion of periodically flood inundation pixels while maintaining an adequate number of observations. Baseline subset selection can be supported by additional data, such as historical hydrographs as reference data. With a GEE workflow, these adjustments do not require major changes to the temporal subset step during baseline statistics computation.

Our study also did not account for flood inundation vegetation. Double-bounce backscatter can be detected using single- or dual-polarized SAR backscatter, allowing positive backscatter changes to be applied (Cian *et al*., 2018). Although White *et al*. (2015) suggest more robust methods to characterize backscatter responses, these approaches rely heavily on complex SAR amplitude and phase data, which are less compatible with the GEE framework (Gorelick *et al*., 2017). Given the abundance of time-series optical imagery and high-level data products, the algorithm in this study could be extended to automatically identify flood inundation in vegetated areas (Sexton *et al*., 2013).

Furthermore, our study did not consider flood inundation in densely built-up areas. This limitation arises from difficulties in extracting reliable backscatter signatures and a lack of strong reference data. These areas are typically characterized by impervious surfaces adjacent to vertical building features, producing high backscatter values even when not flood inundation. Given the high priority of such zones, addressing this issue is a critical challenge. Z-score differences can highlight increased backscatter as a response to flood inundation. A study in western Houston experienced flood inundation in two reservoirs (DeVries *et al*., 2020), and comparison with SkySat imagery obtained the following day confirmed positive Z-scores corresponding to flood inundation pixels (Murthy *et al*., 2014). Future research could integrate these results with high-resolution topographic data and hydraulic models to extend flood inundation prediction to urban areas (Mason *et al*., 2012).

The algorithm is also constrained by the Sentinel-1 satellite revisit period when mapping flood inundation. Flood inundation is highly dynamic, and daily or sub-daily information is often required. Relatively long revisit times in other regions worldwide are insufficient for tracking flood inundation progression. Therefore, higher temporal resolution during critical monitoring periods is needed. Combining contemporaneous Landsat-8 and Sentinel-2 data can improve temporal resolution; however, cloud cover during and after flood inundation events may limit the extent to which these data fill temporal gaps, which is a common challenge. Alternatively, integrating data from other SAR sensors may increase observations during flood events. Sentinel-1 currently offers the most widely accessible SAR dataset fully integrated into GEE. Although other SAR datasets such as ALOS-2 PALSAR-2 or PALSAR Mosaic exist, their availability is limited to specific regions or acquisition modes/polarizations. Additionally, quality, spatial resolution, and preprocessing levels (e.g., calibration, terrain correction, noise reduction) vary across datasets, making Sentinel-1 the primary source for SAR-based modeling and monitoring of flood inundation in GEE.

Another limitation arises because GEE does not yet provide full access to Single Look Complex (SLC) imagery required for interferometric analysis, limiting the application of certain algorithms. Future open-access SAR missions, such as NASA–ISRO SAR (NISAR), which uses longer wavelengths than Sentinel-1, are expected to expand opportunities for multi-mission SAR integration in flood inundation monitoring algorithms. Since our algorithm is designed to adjust sensor bias separately via baseline statistics, future studies anticipate that NISAR data can be seamlessly integrated into existing flood inundation monitoring systems.

CONCLUSIONS

This research shows that the use of the change detection method and the Otsu threshold on multi-temporal Sentinel-1 imagery can extract the extent of flood inundation on 2015, 2020, and 2024 in the Konaweha watershed with an area of up to 6,709.24 ha, 16,295.35 ha, and 9,243.28 ha, respectively. The combination of change detection and machine learning methods using the RF algorithm on Landsat-8 imagery was able to detect LULC changes in the Konaweha Watershed from 2015 to 2024. The decrease in LULC such as wetlands, primary forests, and agriculture, and the increase in built-up areas, bare land, water bodies, secondary forests, bushes, and oil palm plantations indicate environmental degradation in the area. The results of this study also show that LULC changes are correlated with increased flood risk, which has an impact on ecosystems and environmental quality. The Otsu thresholding is able to predict flood inundation using remote sensing data, which can help in disaster monitoring more effectively.

These findings are relevant in the international context as they demonstrate the potential of remote sensing technology in monitoring environmental changes, especially in disaster-prone areas. This study offers new insights in the field of Landscape Ecology, especially related to association between LULC changes and flood risk, rather than direct causation. The integration of these analytical methods can enrich the study of degraded ecosystems and provide very important information for disaster management planning and better natural resource management in the future.

ACKNOWLEDGMENTS

The authors would like to thank the USGS, BPBD, and GEE for providing free data for this research. The authors also expressed his gratitude to the National Disaster Management Agency for providing references and examples of flood disaster data.

CONFLICTS OF INTEREST

The authors declare no conflict of interest.

REFERENCES

Abdo, H. G., (2018). Impacts of war in Syria on vegetation dynamics and erosion risks in Safita area, Tartous, Syria. *Regional environmental change*, 18(6): 1707-1719. https://doi.org/10.1007/s10113-018-1280-3

Acharya, T. D., Subedi, A., Lee, D. H., (2018). Evaluation of water indices for surface water extraction in a Landsat 8 scene of Nepal. *Sensors*, 18(8): 2580. https://doi.org/10.3390/s18082580

Acharya, T. D., Subedi, A., Yang, I. T., Lee, D. H., (2017). Combining water indices for water and background threshold in Landsat image. *Proceedings*, 2(3): 143. https://doi.org/10.3390/ecsa-4-04902

Aghsaei, H., Dinan, N. M., Moridi, A., Asadolahi, Z., Delavar, M., Fohrer, N., Wagner, P. D. (2020). Effects of dynamic land use/land cover change on water resources and sediment yield in the Anzali wetland catchment, Gilan, Iran. *Science of the Total Environment, 712*, 136449. https://doi.org/10.1016/j.scitotenv.2019.136449

Ambari, L.W. (2013). *Indonesia Suffers Sixty Floodings.* Retrieved February 27, 2025, from https://bali.antaranews.com/berita/38426/indonesia-suffers-sixty-floodings

Andono, R. (2014). Studi Penilaian Indikator Kinerja DAS Konaweha Terhadap Perubahan Tata Guna Lahan Berdasarkan Kriteria Hidrologis. (Theses, Brawijaya University). http://repository.ub.ac.id/id/eprint/155836

Antony, N.D. (2020). *BNPB: 50 Desa di Konawe Sultra Terendam Banjir*, 4.046 Jiwa Mengungsi. Retrieved February 27, 2025, from: https://news.detik.com/berita/d-5101856/

bnpb-50-desa-di-konawe-sultra-terendam-banjir-4-046-jiwa-mengungsi?

Arfanuzzaman, M., Dahiya, B, (2019). Sustainable urbanization in Southeast Asia and beyond: Challenges of population growth, land use change, and environmental health. *Growth and Change*, 50(2): 725-744. https://doi.org/10.1111/grow.12297

Aryal, A., Acharya, A., Kalra, A., (2022). Assessing the Implication of Climate Change to Forecast Future Flood Using CMIP6 Climate Projections and HEC-RAS Modeling. *Forecasting*, 4(3): 582-603. https://doi.org/10.3390/forecast4030032

Akaolisa, C. C., Agbasi, O. E., Etuk, S. E., Adewumi, R. O. W. L. A. N. D., Okoli, E. A. (2023). Evaluating the Effects of Real Estate Development in Owerri, Imo State, Nigeria: Emphasizing Changes in Land Use/Land Cover (LULC). *Journal of Landscape Ecology, 16*(2): 98-113. https://doi.org/10.2478/jlecol-2023-0012

Akar, Ö., Güngör, O., (2012). Classification of multispectral images using Random Forest algorithm. *Journal of Geodesy and Geoinformation*, 1(2): 105-112. https://doi.org/10.9733/jgg.241212.1

Amitrano, D., Di Martino, G., Iodice, A., Riccio, D., Ruello, G., (2018). Unsupervised rapid flood mapping using Sentinel-1 GRD SAR images. *IEEE Transactions on Geoscience and Remote Sensing,* 56(6): 3290-3299. https://doi.org/10.1109/TGRS.2018.2797536

Astuti, I. S., Sahoo, K., Milewski, A., Mishra, D. R. (2019). Impact of land use land cover (LULC) change on surface runoff in an increasingly urbanized tropical watershed. *Water Resources Management, 33*(12): 4087-4103. https://doi.org/10.1007/s11269-019-02320-w

Baco, L., Manan, A., Syaf, H., Bana, S. (2021). Analisis Daerah Rawan Banjir dan Tanah Longor di Daerah Aliran Sungai Konaweha Provinsi Sulawesi Tenggara. *Jurnal Perencanaan Wilayah, 6*(1): 93-102. https://doi.org/10.33772/jpw.v6i1.18203

Baccari, N., Hamza, M. H., Slama, T., Sebei, A., Ouerghi, S., Elsheikh, R., ... Elhag, M. (2025). Assessment of Machine Learning Techniques in Mapping Land Use/Land Cover Changes in a Semi-Arid Environment. *Earth Systems and Environment*, 1-21. https://doi.org/10.1007/s41748-024-00562-2

Badan Standardisasi Nasional. (2022). Klasifikasi penutup lahan - Bagian 1: Skala kecil dan menengah. Jakarta: Badan Standardisasi Nasional.

Banjara, M., Bhusal, A., Ghimire, A. B., Kalra, A., (2024). Impact of Land Use and Land Cover Change on Hydrological Processes in Urban Watersheds: Analysis and Forecasting for Flood Risk Management. *Geosciences*, *14*(2): 40. https://doi.org/10.3390/geosciences14020040

Barredo, J. I., Engelen, G. (2010). Land use scenario modeling for flood risk mitigation. *Sustainability, 2*(5): 1327-1344. https://doi.org/10.3390/su2051327

Birhanu, A., Masih, I., Van Der Zaag, P., Nyssen, J., Cai, X. (2019). Impacts of land use and land cover changes on hydrology of the Gumara catchment, Ethiopia. *Physics and Chemistry of the Earth, Parts a/b/c*, 112: 165-174. https://doi.org/10.1016/j.pce.2019.01.006

Boardman, J., Vandaele, K., Evans, R., Foster, I. D. (2019). Off-site impacts of soil erosion and runoff: Why connectivity is more important than erosion rates. *Soil Use and Management, 35*(2): 245-256. https://doi.org/10.1111/sum.12496

BMKG, (2020). *Analisis Dinamika Atmosfer-Laut; Analisis & Prediksi Curah Hujan*. Bidang Analisis Variabilitas Iklim. Pusat Informasi Perubahan Iklim- Kedeputian Bidang Klimatologi.

BNPB, (2021). Kajian Risiko Bencana Nasional Provinsi Sulawesi Tenggara 2022-2026. Jakarta: Badan Nasional Penanggulangan Bencana.

BPS, (2015a). *Jumlah Curah Hujan Menurut Bulan di Provinsi Sulawesi Tenggara (mm), 2015*. Retrieved October 10, 2025, from: https://sultra.bps.go.id/id/statistics-table/1/MzUzIzE=/jumlah-curah-hujan-menurut-bulan-di-provinsi-sulawesi-tenggara-mm-2015.html

BPS, (2015b). *Rata-rata Suhu Udara Menurut Bulan dan Stasiun di Provinsi Sulawesi Tenggara (°C), 2015*. Retrieved October 10, 2025, from: https://sultra.bps.go.id/id/statistics-table/1/MzUxIzE=/rata-rata-suhu-udara-menurut-bulan-dan-stasiun-di-provinsi-sulawesi-tenggara--oc---2015.html

BPS, (2019a). *Jumlah Curah Hujan Menurut Bulan dari Stasiun Pengamatan di Provinsi Sulawesi Tenggara (mm), 2019*. Retrieved October 10, 2025, from: https://sultra.bps.go.id/id/statistics-table/1/MjY4MyMx/jumlah-curah-hujan-menurut-bulan-dari-stasiun-pengamatan-di-provinsi-sulawesi-tenggara--mm---2019.html

BPS, (2019b). *Rata-rata Suhu Udara Menurut Bulan dan Stasiun di Provinsi Sulawesi Tenggara (°C), 2019*. Retrieved October 10, 2025, from: https://sultra.bps.go.id/id/statistics-table/1/MjY4MSMx/rata-rata-suhu-udara-menurut-bulan-dan-stasiun-di-provinsi-sulawesi-tenggara-oc-2019.html

BPS, (2020). *Jumlah Curah Hujan Menurut Bulan dari Stasiun Pengamatan di Provinsi Sulawesi Tenggara (mm), 2020*. Retrieved October 10, 2025, from: https://sultra.bps.go.id/id/statistics-table/1/NDQ0NCMx/jumlah-curah-hujan-menurut-bulan-dari-stasiun-pengamatan-di-provinsi-sulawesi-tenggara--mm---2020.html

BPS, (2023). *Statistik Tanaman Hortikultura Kabupaten Konawe 2022/2023*. Retrieved October 10, 2025, from: konawekab.bps.go.id/publication/2023/12/04/581059998f4e67cbc24a3ca0/statistik-tanaman-hortikultura-kabupaten-konawe-2022-2023.html (accessed 20 May 2024)

Breiman, L. (2001). *Random Forest*. Machine Learning, 5-32.

Calder, I. R., Aylward, B., (2006). Forest and floods: Moving to an evidence-based approach to watershed and integrated flood management. *Water International*, 31(1): 87-99. https://doi.org/10.1080/02508060608691918

Cao, H., Zhang, H., Wang, C., Zhang, B. (2019). Operational flood detection using Sentinel-1 SAR data over large areas. *Water, 11*(4): 786. https://doi.org/10.3390/w11040786

Chaouch, N., Temimi, M., Hagen, S., Weishampel, J., Medeiros, S., Khanbilvardi, R. (2012). A synergetic use of satellite imagery from SAR and optical sensors to improve coastal flood mapping in the Gulf of Mexico. *Hydrological processes, 26*(11): 1617-1628. https://doi.org/10.1002/hyp.8268

Chulafak, G. A., Kushardono, D., Yulianto, F., (2021). Utilization of multi-temporal Sentinel-1 satellite imagery for detecting aquatic vegetation change in Lake Rawapening, Central Java, Indonesia. *Papers in Applied Geography*, 7(3): 316-330. https://doi.org/10.1080/23754931.2021.1890193

Cian, F., Marconcini, M., Ceccato, P. (2018). Normalized Difference Flood Index for rapid flood mapping: Taking advantage of EO big data. *Remote sensing of environment, 209:* 712-730. https://doi.org/10.1016/j.rse.2018.03.006.

Carrasco, L., O'Neil, A. W., Morton, R. D., & Rowland, C. S. (2019). Evaluating Combinations of Temporally Aggregated Sentinel-1, Sentinel-2 and Landsat 8 for Land

Cover Mapping with Google Earth Engine. *Remote Sensing*, 11(3): 288. https://doi.org/10.3390/rs11030288

Dalanhol, I., Tabalipa, N. L., Silva, F. (2020). Future land-use and and-cover scenarios for mapping flood-prone areas in Pato Branco city, Brazil. *In International Congress on Engineering-Engineering for Evolution, KnE Engineering, 2020*: 314-323. https://doi.org/10.18502/keg.v5i6.7049

Deng, Y., Jiang, W., Ling, Z., Wang, X., Peng, K., Li, Z. (2023). Automated and refined wetland mapping of Dongting Lake using migrated training samples based on temporally dense Sentinel 1/2 imagery. *International Journal of Digital Earth, 16*(1): 3199-3221. https://doi.org/10.1080/17538947.2023.2241428

Devi, N. N., Sridharan, B., Kuiry, S. N. **(**2019**)**. Impact of urban sprawl on future flooding in Chennai city, India. *Journal of Hydrology, 574*, 486-496. https://doi.org/10.1016/ j.jhydrol.2019.04.041

DeVries, B., Huang, C., Armston, J., Huang, W., Jones, J. W., Lang, M. W. **(**2020**)**. Rapid and robust monitoring of flood events using Sentinel-1 and Landsat data on the Google Earth Engine. *Remote Sensing of Environment*, 240: 111664. https://doi.org/10.1016/ j.rse.2020.111664

Echendu, A. J., **(**2020**)**. The impact of flooding on Nigeria's sustainable development goals (SDGs). *Ecosystem Health and Sustainability*, 6(1): 1791735. https://doi.org/10.1080/ 20964129.2020.1791735

Erna, E., Muliddin, M., & Harimudin, J. (2021). Analisis Pola dan Intensitas Curah Hujan Berdasarkan Data TRMM di Sulawesi Tenggara. *JAGAT (Jurnal Geografi Aplikasi Dan Teknologi), 5*(2): 105. https://doi.org/10.33772/jagat.v5i2.21465

Faisal, K., Shaker, A., (2017). An investigation of GIS overlay and PCA techniques for urban environmental quality assessment: a case study in Toronto, Ontario, Canada. *Sustainability*, 9(3): 380. https://doi.org/10.3390/su9030380

Gan, B. R., Liu, X. N., Yang, X. G., Wang, X. K., Zhou, J. W. (2018). The impact of human activities on the occurrence of mountain flood hazards: lessons from the 17 August 2015 flash flood/debris flow event in Xuyong County, south-western China. *Geomatics, Natural Hazards and Risk, 9*(1): 816-840. https://doi.org/10.1080/19475705.2018.1480539

Ganaie, T. A., Jamal, S., Ahmad, W. S. (2021). Changing land use/land cover patterns and growing human population in Wular catchment of Kashmir Valley, India. *GeoJournal, 86*, 1589-1606. https://doi.org/10.1007/s10708-020-10146-y

Gatti, R. C., Liang, J., Velichevskaya, A., Zhou, M. (2019). Sustainable palm oil may not be so sustainable. *Science of the Total Environment, 652*, 48-51. https://doi.org/10.1016/j.scitotenv.2018.10.222

Gay, E. T., Martin, K. L., Caldwell, P. V., Emanuel, R. E., Sanchez, G. M., Suttles, K. M. (2023). Riparian buffers increase future baseflow and reduce peakflows in a developing watershed. *Science of the Total Environment, 862*: 160834. https://doi.org/10.1016/ j.scitotenv.2022.160834

Gorelick, N., Hancher, M., Dixon, M., Ilyushchenko, S., Thau, D., Moore, R. (2017). Google Earth Engine: Planetary-scale geospatial analysis for everyone. *Remote sensing of Environment*, 202: 18-27. https://doi.org/10.1016/j.rse.2017.06.031

Handayani, W., Chigbu, U. E., Rudiarto, I., Putri, I. H. S. (2020). Urbanization and Increasing flood risk in the Northern Coast of Central Java—Indonesia: An assessment towards better land use policy and flood management. *Land*, 9(10): 343. https://doi.org/10.3390/land9100343

Hariadi, M. H., Van Der Schrier, G., Steeneveld, G. J., Sutanto, S., Sutanudjaja, E., Ratri, D. N., ... Klein Tank, A. (2023). A high-resolution perspective of extreme rainfall and river flow under extreme climate change in Southeast Asia. *Hydrology and Earth System Sciences Discussions*, 2023, 1-29. https://doi.org/10.5194/hess-28-1935-2024

Hua, A. K. (2017). Land use land cover changes in detection of water quality: a study based on remote sensing and multivariate statistics. *Journal of environmental and public health, 2017*(1), 7515130. https://doi.org/10.1155/2017/7515130

Huang, C., Chen, Y., Zhang, S., Wu, J., (2018a). Detecting, extracting, and monitoring surface water from space using optical sensors: A review. *Reviews of Geophysics*, 56(2): 333-360. https://doi.org/10.1029/2018RG000598

Huang, W., DeVries, B., Huang, C., Lang, M. W., Jones, J. W., Creed, I. F., & Carroll, M. L. (2018b). Automated Extraction of Surface Water Extent from Sentinel-1 Data. *Remote Sensing, 10*(5): 797. https://doi.org/10.3390/rs10050797

Huang, J., Kang, Q., Yang, J. X., Jin, P. W. (2017). Multifactor analysis and simulation of the surface runoff and soil infiltration at different slope gradients. *In IOP Conference Series: Earth and Environmental Science, 82*(1): 012019. https://doi.org/10.1088/1755-1315/82/1/012019

Huang, M., Jin, S., (2020). Rapid flood mapping and evaluation with a supervised classifier and change detection in Shouguang using Sentinel-1 SAR and Sentinel-2 optical data. *Remote Sensing*, *12*(13): 2073. https://doi.org/10.3390/rs12132073

Idowu, D., Zhou, W., (2021). Land use and land cover change assessment in the context of flood hazard in Lagos State, Nigeria. *Water*, *13*(8): 1105. https://doi.org/10.3390/w13081105

Irham, M., Irpan, M., Sartika, D., Setiya Nugraha, G., Dharma, D. B. (2022). Study of the suitability of rock type with the chemical typology of groundwater in the Jeunib basin, Aceh. *Arabian Journal of Geosciences, 15*(3): 220. https://doi.org/10.1007/s12517-022-09489-2

Islam, M. T., Meng, Q. (2022). An exploratory study of Sentinel-1 SAR for rapid urban flood mapping on Google Earth Engine. *International Journal of Applied Earth Observation and Geoinformation, 113*: 103002. https://doi.org/10.1016/j.jag.2022.103002

Iturriza, M., Labaka, L., Ormazabal, M., Borges, M. (2020). Awareness-development in the context of climate change resilience. *Urban Climate, 32*, 100613. https://doi.org/10.1016/j.uclim.2020.100613

Jasman, J., Syarif, M., Sukri, A. S., Ngii, E., Hasddin. (2023). Model of the linkage between land cover changes to water discharge and food productivity: The case of the Konaweha watershed in Indonesia. *Journal of the Geographical Institute" Jovan Cvijic", SASA, 73*(2): 169-185. https://doi.org/10.2298/IJGI2302169M

Jega, A. A., Man, N., Latiff, I. A., Wong, K. K. S. (2018). Flood Disaster Effect on SmallholderFarmers' Food Security inKelantan: An Ordered Logistic Regression Analysis. *IOSR Journal of Agriculture and Veterinary Science (IOSR-JAVS), 11*(3): 42-50. https://doi.org/10.9790/2380-1103024250.

Johary, R., Révillion, C., Catry, T., Alexandre, C., Mouquet, P., Rakotoniaina, S., Pennober, G., & Rakotondraompiana, S. (2023). Detection of Large-Scale Floods Using Google Earth Engine and Google Colab. *Remote Sensing,* 15(22), 5368. https://doi.org/10.3390/rs15225368

Jojon, (2020). Banjir Konawe, 49 Desa Terendam dan 8.314 Jiwa Terdampak. Online: cnnindonesia.com/nasional/20200719001709-20-526282/banjir-konawe-49-desa-terendam-dan-8314-jiwa-terdampak (accessed 3 May 2024)

Jojon., (2022). *Konawe Terendam Banjir, 150 Warga Terdampak*. Retrieved May 3, 2024, from: cnnindonesia.com/nasional/20220802203808-20-829471/konawe-terendam-banjir-150-warga-terdampak

Karlson, M., Bastviken, D. (2023). Multi-Source Mapping of Peatland Types Using Sentinel-1, Sentinel-2, and Terrain Derivatives—A Comparison Between Five High-Latitude Landscapes. *Journal of Geophysical Research: Biogeosciences, 128*(4): e2022JG007195. https://doi.org/10.1029/2022JG007195

Kementerian Pekerjaan Umum**,** (2020). *Banjir DAS Konaweha.* Retrieved February 26 2025, from:: https://sda.pu.go.id/balai/bwssulawesi4/news/banjir-das-konaweha

Kementerian Pekerjaan Umum, (2020b). *Mitigasi Banjir di Sulawesi Tenggara, Ditjen SDA bangun Tanggul dan Kolam Retensi.* Retrieved February 26, 2025, from: https://kabarsulawesi.com/mitigasi-banjir-di-sulawesi-tenggara-ditjen-sda-bangun-tanggul-dan-kolam-retensi/?

Kelley, L. C., Prabowo, A., (2019). Flooding and land use change in Southeast Sulawesi, Indonesia. *Land*, 8(9): 139. https://doi.org/10.3390/land8090139

Kim, S., Sohn, H. G., Kim, M. K., Lee, H. (2019). Analysis of the relationship among flood severity, precipitation, and deforestation in the Tonle Sap Lake Area, Cambodia Using Multi-Sensor approach. *KSCE Journal of Civil Engineering, 23*(3): 1330-1340. https://doi.org/10.1007/s12205-019-1061-7

Kundzewicz, Z. W., Kanae, S., Seneviratne, S. I., Handmer, J., Nicholls, N., Peduzzi, P., ... Sherstyukov, B. (2014). Flood risk and climate change: global and regional perspectives. *Hydrological Sciences Journal, 59*(1), 1-28. https://doi.org/10.1080/02626667.2013.857411

Lacher, I. L., Ahmadisharaf, E., Fergus, C., Akre, T., Mcshea, W. J., Benham, B. L., Kline, K. S. (2019). Scale-dependent impacts of urban and agricultural land use on nutrients, sediment, and runoff. *Science of the Total Environment, 652*, 611-622. https://doi.org/10.1016/j.scitotenv.2018.09.370

Lang, F., Zhu, Y., Zhao, J., Hu, X., Shi, H., Zheng, N., Zha, J. (2024). Flood Mapping of Synthetic Aperture Radar (SAR) Imagery Based on Semi-Automatic Thresholding and Change Detection. *Remote Sensing, 16*(15): 2763. https://doi.org/10.3390/rs16152763

Lechner, A. M., Foody, G. M., Boyd, D. S., (2020). Applications in remote sensing to forest ecology and management. *One Earth, 2*(5): 405-412. https://doi.org/10.1016 /j.oneear.2020.05.001

Lee, Y., Brody, S. D., (2018). Examining the impact of land use on flood losses in Seoul, Korea. *Land use policy*, 70: 500-509. https://doi.org/10.1016/j.landusepol.2017.11.019

Lestari, S., King, A., Vincent, C., Karoly, D., Protat, A. (2019). Seasonal dependence of rainfall extremes in and around Jakarta, Indonesia. *Weather and Climate Extremes, 24*, 100202. https://doi.org/10.1016/j.wace.2019.100202

Li, J., Peng, B., Wei, Y., Ye, H., (2021a). Accurate extraction of surface water in complex environment based on Google Earth Engine and Sentinel-2. *PloS one*, *16*(6): e0253209. https://doi.org/10.1371/journal.pone.0253209

Li, X., Zhang, Y., Ma, N., Li, C., Luan, J. (2021b). Contrasting effects of climate and LULC change on blue water resources at varying temporal and spatial scales. *Science of The Total Environment, 786*, 147488. https://doi.org/10.1016/j.scitotenv.2021.147488

Liping, C., Yujun, S., Saeed, S. (2018). Monitoring and predicting land use and land cover changes using remote sensing and GIS techniques—A case study of a hilly area, Jiangle, China. *PloS one, 13*(7): e0200493. https://doi.org/10.1371/journal.pone.0200493

Loc, H. H., Park, E., Chitwatkulsiri, D., Lim, J., Yun, S. H., Maneechot, L. (2020). Local rainfall or river overflow? Re-evaluating the cause of the Great 2011 Thailand flood. *Journal of Hydrology,* 589, 125368. https://doi.org/10.1016/j.jhydrol.2020.125368

Maladeni, E. S., Haydir, H., Jasman, O. O. H. (2023). Monitoring of River Water Discharge Volume in the Konaweha Watershed, Southeast Sulawesi Province, Indonesia. *International Journal of Recent Engineering Science, 10*(5): 24-29. https://doi.org/10.14445/23497157/IJRES-V10I5P103

Manjusree, P., Prasanna Kumar, L., Bhatt, C. M., Rao, G. S., Bhanumurthy, V. (2012). Optimization of threshold ranges for rapid flood inundation mapping by evaluating backscatter profiles of high incidence angle SAR images. *International Journal of Disaster Risk Science, 3*(2): 113-122. https://doi.org/10.1007/s13753-012-0011-5

Martinis, S., Twele, A., Strobl, C., Kersten, J., Stein, E. (2013). A multi-scale flood monitoring system based on fully automatic MODIS and TerraSAR-X processing chains. *Remote Sensing, 5*(11): 5598-5619. https://doi.org/10.3390/rs5115598

Marwah, S. (2014). Analisis Perubahan Penggunaan Lahan dan Ketersediaan Sumberdaya Air di DAS Konaweha Provinsi Sulawesi Tenggara. *Jurnal Agroteknos, 4*(3): 208-2018.

Mason, D. C., Davenport, I. J., Neal, J. C., Schumann, G. J. P., Bates, P. D. (2012). Near real-time flood detection in urban and rural areas using high-resolution synthetic aperture radar images. *IEEE transactions on Geoscience and Remote Sensing, 50*(8), 3041-3052. https://doi.org/10.1109/TGRS.2011.2178030.

Mehr, A. D., Akdegirmen, O. (2021). Estimation of urban imperviousness and its impacts on flashfloods in Gazipaşa, Turkey. *Knowledge-Based Engineering and Sciences, 2*(1): 9-17. https://doi.org/10.51526/kbes.2021.2.1.9-17

Meyers, S. D., Landry, S., Beck, M. W., Luther, M. E. (2021). Using logistic regression to model the risk of sewer overflows triggered by compound flooding with application to sea level rise. *Urban Climate, 35*, 100752. https://doi.org/10.1016/j.uclim.2020.100752

McHugh, M. L., (2012). Lessons in biostatistics interrater reliability: the kappa statistic. *Biochemica Medica, 22*(3): 276-282. https://pub-med.ncbi.nlm.gov/23092060/

Moharrami, M., Javanbakht, M., Attarchi, S. (2021). Automatic flood detection using sentinel-1 images on the google earth engine. *Environmental monitoring and assessment, 193*(5): 248. https://doi.org/10.1007/s10661-021-09037-7

Morse, I. (2019). Indonesian flooding disaster bears the hallmarks of agriculture and mining impact. Retrieved February 26, 2025, from: https://news.mongabay.com/2019/08/in-sulawesi-floods-bear-the-hallmarks-of-agriculture-and-mining-impacts/?

Mukaddas, J., Iswandi, M., Syaf, H., Yusuf, D. N., (2023). Spatial Pattern Modeling of Sustainable Mining Industrial Area in Routa of Konawe Regency, Southeast Sulawesi Province. *RES MILITARIS*, *13*(3): 2785-2793.

Murthy, K., Shearn, M., Smiley, B. D., Chau, A. H., Levine, J., Robinson, M. D. (2014). October. SkySat-1: very high-resolution imagery from a small satellite. *In Sensors, systems, and next-generation Satellites XVIII, 9241*: 367-378. https://doi.org/10.1117/12.2074163.

Naikoo, M. W., Rihan, M., Ishtiaque, M. (2020). Analyses of land use land cover (LULC) change and built-up expansion in the suburb of a metropolitan city: Spatio-temporal analysis of Delhi NCR using landsat datasets. *Journal of Urban Management, 9*(3): 347-359. https://doi.org/10.1016/j.jum.2020.05.004

Nie, C., Li, H., Yang, L., Wu, S., Liu, Y., Liao, Y., (2012). Spatial and temporal changes in flooding and the affecting factors in China. *Natural Hazards*, 61: 425-439. https://doi.org/10.1007/s11069-011-9926-1

Nguyen, A. H., Nguyen, P. T., Nguyen, T. T. (2023). Enhanced flood water depth estimation from Sentinel-1A images. *International Journal of Remote Sensing, 44*(20): 6399-6421. https://doi.org/10.1080/01431161.2023.2268819

Nguyen, H. T. T., Doan, T. M., Tomppo, E., McRoberts, R. E., (2020). Land Use/land cover mapping using multitemporal Sentinel-2 imagery and four classification methods—A case study from Dak Nong, Vietnam. *Remote Sensing*, 12(9): 1367. https://doi.org/10.3390/rs12091367

Ochoa-Sánchez, A. E., Crespo, P., Carrillo-Rojas, G., Marín, F., Célleri, R. (2020). Unravelling evapotranspiration controls and components in tropical Andean tussock grasslands. *Hydrological Processes, 34*(9): 2117-2127. https://doi.org/10.1002/hyp.13716

Oda, T., Egusa, T., Ohte, N., Hotta, N., Tanaka, N., Green, M. B., Suzuki, M. (2021). Effects of changes in canopy interception on stream runoff response and recovery following clear-cutting of a Japanese coniferous forest in Fukuroyamasawa Experimental Watershed in Japan. *Hydrological Processes, 35*(5): e14177. https://doi.org/10.1002/hyp.14177

Otsu, N. (1975). A threshold selection method from gray-level histograms. *Automatica, 11*(285-296): 23-27.

Özelkan, E., (2020). Water body detection analysis using NDWI indices derived from landsat-8 OLI. *Polish Journal of Environmental Studies*, 29(2): 1759-1769. https://doi.org/10.15244/pjoes/110447

Papila, I., Alganci, U., & Sertel, E. (2020). Sentinel-1 based flood mapping using interferometric coherence and intensity change detection approach. *The International Archives of the Photogrammetry, Remote Sensing and Spatial Information Sciences, 43*, 1697-1703. https://doi.org/10.5194/isprs-archives-XLIII-B3-2020-1697-2020

Pati, K. A. (2013). Banjir di Konawe, Dua Tewas dan 22 Kecamatan Terendam. Retrieved February 26, 2025, from: https://regional.kompas.com/read/2013/07/19/0924390/Banjir.di.Konawe.Dua.Tewas.dan.22.Kecamatan.Terendam?

Pedregosa, F., Varoquaux, G., Gramfort, A., Michel, V., Thirion, B., Grisel, O., ... Duchesnay, É. (2011). Scikit-learn: Machine learning in Python. *the Journal of machine Learning research*, 12, 2825-2830.

Pelckmans, I., Belliard, J. P., Gourgue, O., Dominguez-Granda, L. E., Temmerman, S. (2024). Mangroves as nature-based mitigation for ENSO-driven compound flood risks in a large river delta. *Hydrology and Earth System Sciences, 28*(6): 1463-1476. https://doi.org/10.5194/hess-28-1463-2024

Pelletier, C., Valero, S., Inglada, J., Champion, N., Dedieu, G., (2016). Assessing the robustness of Random Forests to map land cover with high resolution satellite image time series over large areas. *Remote Sensing of Environment*, 187: 156-168. https://doi.org/10.1016/j.rse.2016.10.010

Peña-Luque, S., Ferrant, S., Cordeiro, M. C. R., Ledauphin, T., Maxant, J., & Martinez, J.-M. (2021). Sentinel-1&2 Multitemporal Water Surface Detection Accuracies, Evaluated at Regional and Reservoirs Level. *Remote Sensing*, 13(16), 3279. https://doi.org/10.3390/rs13163279

Pham-Duc, B., Prigent, C., Aires, F. (2017). Surface water monitoring within Cambodia and the Vietnamese Mekong Delta over a year, with Sentinel-1 SAR observations. *Water, 9*(6): 366. https://doi.org/10.3390/w9060366

Plank, S. (2014). Rapid damage assessment by means of multi-temporal SAR—A comprehensive review and outlook to Sentinel-1. *Remote Sensing, 6(*6): 4870-4906. https://doi.org/10.3390/rs6064870

Pradhan-Salike, I., Pokharel, J. R. (2017). Impact of urbanization and climate change on urban flooding: A case of the Kathmandu Valley. *JNRD-Journal of Natural Resources and Development*, 7: 56-66. https://doi.org/10.5027/jnrd.v7i0.07

Priyatna, M., Wijaya, S.K., Khomarudin, M.R., Yulianto, F., Nugroho, G., Afgatiani, P.M., Rarasati, A. Hussein, M.A. (2023). Use of multi-sensor satellite imagery to analyze flood events and land cover changes using change detection and machine learning techniques in the Barito watershed. *Journal of Degraded and Mining Lands Management, 10*(2):4073-4080. https://doi.org/10.15243/jdmlm.2023.102.4073.

Pumo, D., Arnone, E., Francipane, A., Caracciolo, D., Noto, L. V., (2017). Potential implications of climate change and urbanization on watershed hydrology. *Journal of Hydrology*, 554: 80-99. https://doi.org/10.1016/j.jhydrol.2017.09.002

Puno, G. R., Puno, R. C. C., (2019). Watershed conservation prioritization using geomorphometric and land use-land cover parameters. *Global Journal of Environmental Science and Management*, *5*(3): 279-294. https://doi.org/10.22034/GJESM.2019.03.02

Purinton, B., Bookhagen, B., (2020). Multiband (X, C, L) radar amplitude analysis for a mixed sand-and gravel-bed river in the eastern Central Andes. *Remote sensing of environment,* 246: 111799. https://doi.org/10.1016/j.rse.2020.111799

Rakyat, H., (2020). *Banjir Landa Konawe, 4 Ribu Jiwa di 50 Desa jadi Korban*. Retrieved May 3, 2025, from: haluanrakyat.com/banjir-landa-konawe-4-ribu-jiwa-di-50-desa-jadi -korban

Ramakrishna, G., Gaddam, S. R., Daisy, I. (2014). Impact of floods on food security and livelihoods of IDP tribal households: The case of Kham-mam region of India. *International Journal of Development and Economics Sustainability*, *2*(1): 11-24.

Rahmoun, T., Zhao, W., Hammad, M., Hassan, M., (2018). Ruralization vs. Urbanization Sprawl as Guiding Regional Planning: Development Scenario for Rivers Watershed in the Southern Syrian Coastal Region. *IOP Conference Series: Earth and Environmental Science*, 151: 012033. https://doi.org/10.1088/1755-1315/151/1/012033

Rawat, J. S., Kumar, M. (2015). Monitoring land use/cover change using remote sensing and GIS techniques: A case study of Hawalbagh block, district Almora, Uttarakhand, India. *The Egyptian Journal of Remote Sensing and Space Science, 18*(1), 77-84. https://doi.org/10.1016/j.ejrs.2015.02.002

Reed, C., Anderson, W., Kruczkiewicz, A., Nakamura, J., Gallo, D., Seager, R., McDermid, S. S. (2022). The impact of flooding on food security across Africa. *Proceedings of the National Academy of Sciences, 119*(43): e2119399119. https://doi.org/10.1073/pnas.2119399119

Rucci, A., Ferretti, A., Guarnieri, A. M., Rocca, F. (2012). Sentinel 1 SAR interferometry applications: The outlook for sub millimeter measurements. *Remote Sensing of Environment, 120*, 156-163. https://doi.org/10.1016/j.rse.2011.09.030

Sadeghi, S.M.M., Gordon, D.A., Van Stan, J.T., (2020). A Global Synthesis of Throughfall and Stemflow Hydrometeorology. In Precipitation Partitioing by Vegetation: A Global Synthesis; Van Stan, I., John, T., Gutmann, E., Friesen, J., (Eds), *Springer International Publishing*: Cham, Switzerland: 49–70.

Sahoo, S., Dhar, A., Debsarkar, A., Kar, A. **(**2018**)**. Impact of water demand on hydrological regime under climate and LULC change scenarios. *Environmental Earth Sciences*, 77, 1-19. https://doi.org/10.1007/s12665-018-7531-2

Setiawan, K., (2021). *Konaweha Watershed Floods Cause Analysis*. (Undergraduate theses, University of Indonesia). https://lib.ui.ac.id/m/detail.jsp?id=20525080&lokasi=loka

Sexton, J. O., Song, X. P., Feng, M., Noojipady, P., Anand, A., Huang, C., ... Townshend, J. R. (2013). Global, 30-m resolution continuous fields of tree cover: Landsat-based rescaling of MODIS vegetation continuous fields with lidar-based estimates of error. *International Journal of Digital Earth, 6*(5): 427-448. https://doi.org/10.1080/17538947.2013.786146.

Shen, X., Anagnostou, E. N., Allen, G. H., Brakenridge, G. R., Kettner, A. J. (2019). Near-real-time non-obstructed flood inundation mapping using synthetic aperture radar. *Remote Sensing of Environment*, 22: 302-315. https://doi.org/10.1016/j.rse.2018.11.008

Shimada, M., Itoh, T., Motooka, T., Watanabe, M., Shiraishi, T., Thapa, R., Lucas, R. (2014). New global forest/non-forest maps from ALOS PALSAR data (2007–2010). *Remote Sensing of environment, 155*: 13-31. https://doi.org/10.1016/j.rse.2014.04.014

Silva, J. F. C. B. D. C., da Silva, R. M., Santos, C. A. G., Silva, A. M., Vianna, P. C. G. (2021). Analysis of the response of the Epitácio Pessoa reservoir (Brazilian semiarid region) to potential future drought, water transfer and LULC scenarios. *Natural Hazards, 108*, 1347-1371. https://doi.org/10.1007/s11069-021-04736-3

Singha, M., Dong, J., Sarmah, S., You, N., Zhou, Y., Zhang, G., ... Xiao, X. (2020). Identifying floods and flood-affected paddy rice fields in Bangladesh based on Sentinel-1 imagery and Google Earth Engine. *ISPRS Journal of Photogrammetry and Remote Sensing, 166*: 278-293. https://doi.org/10.1016/j.isprsjprs.2020.06.011

Smith, P., Cotrufo, M. F., Rumpel, C., Paustian, K., Kuikman, P. J., Elliott, J. A., ... Scholes, M. C. (2015). Biogeochemical cycles and biodiversity as key drivers of ecosystem services provided by soils. *Soil, 1*(2): 665-685. https://doi.org/10.5194/soil-1-665-2015

Soulibouth, L., Hwang, H. S., Shin, D. H. (2021). The impact of flood damage on farmers, agricultural sector and food security in Laos: A regional case study of Champhone District, Savannaket Province. *Journal of International Development Cooperation, 16*(2): 151-170. https://doi.org/10.34225/jidc.2021.16.2.151

Srivastava, A., Kumari, N., Maza, M. (2020). Hydrological response to agricultural land use heterogeneity using variable infiltration capacity model. *Water Resources Management, 34*(12): 3779-3794. https://doi.org/10.1007/s11269-020-02630-4

Sun, X., Li, X., Tan, B., Gao, J., Wang, L., Xiong, S. (2025). Integrating Otsu Thresholding and Random Forest for Land Use/Land Cover (LULC) Classification and Seasonal Analysis of Water and Snow/Ice. *Remote Sensing, 17*(5): 797. https://doi.org/10.3390/rs17050797

Supari, S. (2012). *Spatiotemporal characteristics of extreme rainfall events over Java Island*, Indonesia (Master's thesis, University of Twente).

Surya, R. A., Purwanto, M. Y. J., Asep Sapei, W. (2014). Tank Model to See The Effect of Land Use Changes on Runoff, Infiltration and Groundwater in SubWatershed of Konaweha South East Sulawesi Indonesia. *Journal of Environment and Earth Science, 4*(14): 107-117.

Tabari, H. (2020). Climate change impact on flood and extreme precipitation increases with water availability. *Scientific reports*, *10*(1): 13768. https://doi.org/10.1038/s41598-020-70816-2

Talukdar, S., Singha, P., Mahato, S., Pal, S., Liou, Y. A., Rahman, A., (2020). Land-use land-cover classification by machine learning classifiers for satellite observations—A review. *Remote Sensing*, *12*(7): 1135. https://doi.org/10.3390/rs12071135

Tamenk, F., (2021). *Banjir Landa Konawe, Puluhan Rumah dan Lahan Pertanian Terendam*. Retrieved May 3, 2024, from: daerah.sindonews.com/read/518098/174/banjir-landa-konawe-puluhan-rumah-dan-lahan-pertanian-terendam-1629594531

Tanika, L. (2013). Dampak Perubahan Tutupan Lahan Dan Iklim Terhadap Fungsi Hidrologi Daerah Aliran Sungai Konaweha Hulu. *Jurnal Sumber Daya Air, 9*(2): 155-168. https://doi.org/10.32679/jsda.v9i2.156

Tang, Y., Leon, A. S., Kavvas, M. L., (2020). Impact of dynamic storage management of wetlands and shallow ponds on watershed-scale flood control. *Water resources management*, 34: 1305-1318. https://doi.org/10.1007/s11269-020-02502-x

Tarpanelli, A., Mondini, A. C., & Camici, S. (2022). *Effectiveness of Sentinel-1 and Sentinel-2 for flood detection assessment in Europe*. Natural Hazards and Earth System Sciences, 22(8), 2473-2489. https://doi.org/10.5194/nhess-22-2473-2022

Tavus, B., Kocaman, S., Gokceoglu, C. (2022). Flood damage assessment with Sentinel-1 and Sentinel-2 data after Sardoba dam break with GLCM features and Random Forest method. *Science of The Total Environment, 816*: 151585. https://doi.org/10.1016/j.scitotenv.2021.151585

Tessler, Z. D., Vörösmarty, C. J., Grossberg, M., Gladkova, I., Aizenman, H., Syvitski, J. P., Foufoula-Georgiou, E. (2015). Profiling risk and sustainability in coastal deltas of the world. *Science*, *349*(6248): 638-643. https://doi.org/10.1126/science.aab3574

Tiede, D., (2014). A new geospatial overlay method for the analysis and visualization of spatial change patterns using object-oriented data modeling concepts. *Cartography and Geographic Information Science*, *41*(3): 227-234. https://doi.org/10.1080/15230406.2014.901900

Torre Zaffaroni, P., Baldi, G., Texeira, M., Di Bella, C. M., Jobbágy, E. G. (2023). The timing of global floods and its association with climate and topography. *Water Resources Research, 59*(7), e2022WR032968. https://doi.org/10.1029/2022WR032968

Tran, K. H., Menenti, M., Jia, L. (2022). Surface Water Mapping and Flood Monitoring in the Mekong Delta Using Sentinel-1 SAR Time Series and Otsu Threshold. *Remote Sensing, 14*(22): 5721. https://doi.org/10.3390/rs14225721

Triet, N. V. K., Dung, N. V., Hoang, L. P., Le Duy, N., Tran, D. D., Anh, T. T., ... Apel, H. (2020). Future projections of flood dynamics in the Vietnamese Mekong Delta. *Science of the Total Environment*, 742, 140596. https://doi.org/10.1016/j.scitotenv.2020.140596

Uddin, K., Matin, M. A., Meyer, F. J., (2019). Operational flood mapping using multi-temporal Sentinel-1 SAR images: A case study from Bangladesh. *Remote Sensing*, *11*(13): 1581. https://doi.org/10.3390/rs11131581

Wang, Y., Li, C., Liu, M., Cui, Q., Wang, H., Jianshu, L. V., ... Hu, Y., (2022). Spatial characteristics and driving factors of urban flooding in Chinese megacities. *Journal of Hydrology*, 613: 128464. https://doi.org/10.1016/j.jhydrol.2022.128464

Westerhoff, R. S., Kleuskens, M. P. H., Winsemius, H. C., Huizinga, H. J., Brakenridge, G. R., Bishop, C. (2013). Automated global water mapping based on wide-swath orbital synthetic-aperture radar. *Hydrology and Earth System Sciences, 17*(2): 651-663. https://doi.org/10.5194/hess-17-651-2013

White, L., Brisco, B., Dabboor, M., Schmitt, A., Pratt, A. (2015). A collection of SAR methodologies for monitoring wetlands. *Remote sensing, 7*(6): 7615-7645. https://doi.org/10.3390/rs70607615.

Vaezi, A. R., Bahrami, H. A., Sadeghi, S. H. R., Mahdian, M. H. (2010). Modeling relationship between runoff and soil properties in dry-farming lands, NW Iran. *Hydrology and Earth System Sciences Discussions, 7*(2): 2577-2607. https://doi.org/10.5194/hessd-7-2577-2010, 2010.

van Heerwaarden, C. C., Guerau de Arellano, J. V. (2008). Relative humidity as an indicator for cloud formation over heterogeneous land surfaces. *Journal of the Atmospheric Sciences, 65*(10): 3263-3277. https://doi.org/10.1175/2008JAS2591.1

Veettil, B. K., Quang, N. X., Trang, N. T. T. (2019). Changes in mangrove vegetation, aquaculture and paddy cultivation in the Mekong Delta: A study from Ben Tre Province, southern Vietnam. *Estuarine, Coastal and Shelf Science, 226*, 106273. https://doi.org/10.1016/j.ecss.2019.106273

Wania, A., Joubert-Boitat, I., Dottori, F., Kalas, M., Salamon, P. (2021). Increasing Timeliness of Satellite-Based Flood Mapping Using Early Warning Systems in the Copernicus Emergency Management Service. *Remote Sensing, 13*(11): 2114. https://doi.org/10.3390/rs13112114

Witanto**,** (2019). Banjir Konawe, 8 Ribu Warga Mengungsi, 25 Kecamatan Terendam. Retrieved May 3, 2025, from: ngopibareng.id/read/banjir-konawe-8-ribu-warga-mengungsi -25-kecamatan-terendam-0

Yin, J., He, F., Xiong, Y. J., Qiu, G. Y., (2017). Effects of land use/land cover and climate changes on surface runoff in a semi-humid and semi-arid transition zone in northwest China. *Hydrology and Earth System Sciences*, 21(1): 183-196. https://doi.org/10.5194/hess-21 -183-2017

Zhang, M., Chen, F., Liang, D., Tian, B., Yang, A., (2020). Use of Sentinel-1 GRD SAR images to delineate flood extent in Pakistan. *Sustainability*, *12*(14): 5784. https://doi.org/10.3390/su12145784

Zhang, M., Li, Z., Tian, B., Zhou, J., Tang, P., (2016). The backscattering characteristics of wetland vegetation and water-level changes detection using multi-mode SAR: A case study. *International Journal of Applied Earth Observation and Geoinformation*, *45*: 1-13. https://doi.org10.1016/j.jag.2015.10.001

Zhang, J., Liu, X., Qin, Y., Fan, Y., Cheng, S. (2024). Wetlands Mapping and Monitoring with Long-Term Time Series Satellite Data Based on Google Earth Engine, Random Forest, and Feature Optimization: A Case Study in Gansu Province, China. *Land, 13*(9), 1527. https://doi.org/10.3390/land13091527

Zhang, X., Liu, L., Zhao, T., Chen, X., Lin, S., Wang, J., ... Liu, W. (2022). GWL_FCS30: global 30 m wetland map with fine classification system using multi-sourced and time-series remote sensing imagery in 2020. *Earth System Science Data Discussions*, 2022, 1-31. https://doi.org/10.5194/essd-15-265-2023

APPENDIX

Table A: Cross-tabulation error matrix of classified vs reference data in the Konaweha watershed

2015										
Classified Data	**Reference Data**									
	BU	**BL**	**WB**	**WL**	**PF**	**SF**	**SR**	**PO**	**AC**	**Total**	**UA**
BU	102	0	0	13	0	0	10	0	96	221	46.15
BL	0	73	0	0	0	0	0	0	0	73	100
WB	0	0	190	0	0	0	0	0	31	221	85.97
WL	0	0	0	79	0	0	0	0	23	102	77.45
PF	0	0	0	0	10899	16	0	0	0	10915	99.85
SF	0	0	0	0	168	650	0	35	0	853	76.20
SR	0	0	0	0	0	7	35	0	0	42	83.33
PO	0	0	0	0	0	1	0	38	0	39	97.44
AC	0	0	5	10	0	9	1	1	250	276	90.58
Total	102	73	195	102	11067	683	46	74	400	12316	
PA	100	90.12	100	86.67	100	40	98.63	45.40	54.17		
Overall Accuracy (OA) 96.65%					Kappa Coefficient 0.86						
2020											
Classified Data	**Reference Data**										
	BU	**BL**	**WB**	**WL**	**PF**	**SF**	**SR**	**PO**	**AC**	**Total**	**UA**
BU	137	0	0	0	0	0	0	0	0	137	100
BL	3	30	0	0	0	0	0	0	0	33	90.91
WB	0	0	27	0	0	0	0	0	0	27	100
WL	0	0	0	10	0	1	0	0	14	16	40
PF	0	0	0	0	14778	268	0	0	0	15046	98.22
SF	0	0	0	0	0	197	0	0	0	197	100
SR	1	0	0	0	0	19	284	4	1	309	91.91
PO	0	0	0	0	0	5	0	56	0	101	91.80
AC	3	0	0	7	0	0	1	2	82	95	86.32
Total	144	30	27	8	14778	490	285	62	97	15592	
PA	95.14	100	100	58.82	100	40.20	99.65	90.32	84.54		
Overall Accuracy (OA) 97.93					Kappa Coefficient 0.83						
2024											
Classified Data	**Reference Data**										
	BU	**BL**	**WB**	**WL**	**PF**	**SF**	**SR**	**PO**	**AC**	**Total**	**UA**
BU	137	0	0	0	0	0	0	0	0	137	100
BL	0	31	0	0	0	1	1	0	0	33	93.94
WB	0	0	317	0	0	0	13	0	14	344	92.15
WL	0	0	0	39	0	15	0	0	1	55	70.91
PF	0	0	0	0	14829	216	0	0	0	15045	98.56
SF	0	0	0	0	0	197	0	0	0	197	100
SR	1	0	1	0	0	20	232	0	56	310	74.84
PO	0	0	0	0	0	5	0	61	0	66	92.42
AC	0	1	0	16	0	4	11	4	59	95	62.11
Total	138	32	318	55	14829	458	257	65	130	15902	
PA	99.28	96.88	99.69	70.91	100	43.01	90.27	93.85	45.38		
Overall Accuracy (OA) 97.66					Kappa Coefficient 0.85						